Cohesin residency determines chromatin loop patterns

Lorenzo Costantino 1*, Tsung-Han S. Hsieh 1*, Rebecca Lamothe 1, Xavier Darzacq 1 and Douglas Koshland 1

1 Department of Molecular and Cell Biology, University of California, Berkeley, Berkeley, CA 94720, USA
*** First co-author**

ABSTRACT: The organization of chromatin into higher-order structures is essential for chromosome segregation, the repair of DNA damage, and the regulation of gene expression. These structures are formed by the evolutionarily conserved SMC (structural maintenance of chromosomes) complexes. By analyzing synchronized populations of budding yeast with Micro-C, we observed that chromatin loops are formed genome-wide, and are dependent upon the SMC complex, cohesin. We correlated the loop signal with the position and intensity of cohesin binding to chromosomes in wild-type and cells depleted for the cohesin regulators Wpl1p and Pds5p. We generate a model to explain how the genomic distribution and frequency of loops are driven by cohesin residency on chromosomes. In this model a dynamic pool of cohesin with loop extrusion activity stops when encountering two regions occupied by stably bound cohesin, forming a loop. Different regions are occupied by cohesin in different cells, defining various patterns of chromatin loops.

INTRODUCTION

The genome is organized into three-dimensional structures that are essential for the correct segregation of chromosomes, the efficient repair of DNA damage, and the regulation of gene transcription. The initial existence of higher-order chromosome structures was discovered in the early 1900s by the dramatic cytological appearance of pairs of condensed sister chromatids in mitosis. Moreover, electron microscopy studies showed that mitotic and meiotic chromatin is organized in loops with a protein scaffold (Gall and Callan, 1962; Marsden and Laemmli, 1979; Paulson and Laemmli, 1977)

A high-resolution view of chromosome folding became possible with the development of new methods based on chromosome conformation capture (3C) technology (Dekker et al., 2002; Denker and de Laat, 2016; Kempfer and Pombo, 2020; Lieberman-Aiden et al., 2009). Essentially, 3Cs methods stabilize the interactions between different regions of the chromatin that are in close spatial proximity, detect these interactions, and visualize them on a contact map. These methods showed the existence of chromatin loops in interphase mammalian cells first at specific loci, then genome-wide (Deng et al., 2012; Palstra et al., 2003; Rao et al., 2014; Tolhuis et al., 2002). Moreover, 3Cs methods showed that mammalian chromosomes are organized into self-associating domains, which contain sequences that are more likely to interact with each other than with the rest of the genome (Dixon et al., 2012; Nora et al., 2012; Sexton et al., 2012). The existence of these loops has inspired several outstanding questions, including what are the molecular mechanisms that drive the formation of loops, their genome distribution, their frequency in a population of cells, and what are the biological function(s) of loops?

A major advance came with the discovery that loop formation depended upon the evolutionarily conserved SMC (structural maintenance of chromosomes) complexes (Sanborn et al., 2015; Wang et al., 2017). SMC complexes can tether together two regions of DNA, either within a single DNA molecule or between DNA molecules (Hassler et al., 2018; Onn et al., 2008). Additionally, they can translocate along DNA to extrude DNA loops (loop extrusion) in vitro and in vivo (Davidson et al., 2019; Ganji et al., 2018; Kim et al., 2019). Loop formation by one SMC complex, called cohesin, has been extensively studied in mammalian cells (Hadjur et al., 2009; Parelho et al., 2008; Wendt et al., 2008). The formation of cohesin-dependent loops also requires the CTCF DNA binding factor (Handoko et al., 2011; Li et al., 2012; Splinter et al., 2006), which colocalizes with cohesin at the base of loops. Cohesin-dependent loops occur preferentially between the two CTCF binding sites that are in a convergent orientation (Guo et al., 2015; Rao et al., 2014; de Wit et al., 2015). Cohesin-dependent loops occurred between more distal CTCF binding sites when the cohesin regulator WAPL was depleted, showing that WAPL restricts loop size. WAPL dissociates cohesin from chromosomes (Haarhuis et al., 2017), and by preventing WAPL binding to cohesin, CTCF is thought to protect the translocating cohesin (Li et al., 2020). The formation of specific loops by cohesin, CTCF, and WAPL has been proposed to contribute to the regulation of gene expression by controlling the interactions of enhancers with distal promoters (Schoenfelder and Fraser, 2019).

However, five observations paint a more complicated picture of the regulation and function of cohesin-dependent looping. First, robust loops still form when the orientation preference of CTCF sites was eliminated through depletion of a cohesin regulator (Wutz et al., 2017). Clearly orientation is not the only determinant of loop position in mammals. Indeed, looping is observed in organisms that do not have the CTCF factor (Heger et al., 2012; Rowley et al., 2020). Thus, fundamental mechanism(s) of positioning loops in most organisms including mammals remains to be determined. Second, a cohesin auxiliary factor, PDS5, facilitates WAPL's ability to remove cohesin from chromosomes, yet the impact of WAPL and PDS5 on looping appear to be different (Wutz et al., 2017). This observation suggests that cohesin regulators control looping by additional yet to be discovered mechanisms. Third, the current understanding of

cohesin, CTCF, WAPL, and PDS5 does not explain why the frequency of loops at different genomic positions can vary dramatically in a cell population (Haarhuis et al., 2017; Wutz et al., 2017). Fourth, current models do not take into account the existence of pools of cohesin that are either dynamically or stably bound to chromosomes. Fifth, the postulated function of looping in gene expression does not explain why most regions of the mammalian genome have cohesin-dependent loops, yet the proper expression of most genes is cohesin/CTCF independent (Nora et al., 2017; Rao et al., 2017; Schwarzer et al., 2017). These observations show that key aspects of the molecular mechanisms and biological function of looping remain to be elucidated

A deep understanding of other complicated cellular processes often resulted from their study in multiple diverse organisms. Indeed loop formation in yeast was analyzed with a high-throughput 3C-method called Hi-C. These studies showed the presence of cohesin-dependent loops (Schalbetter et al., 2017, 2019) whose size was restricted by Wlp1p as observed in mammalian cells (yeast ortholog of WAPL) (Dauban et al., 2020). However, the loop signal in yeast was weak compared to mammalian cells, hindering a deeper understanding of the molecular mechanisms that impact the genomic distribution, and frequency of loops. The weak signal for loops in yeast might have been a reflection of a biological difference between yeast and mammalian cells or methodological limitations of these studies.

We reasoned that previous studies failed to detect strong loop signals in dividing budding yeast because they did not take into account that loops would be small and cell cycle regulated. Micro-C, another 3C-method, has improved the potential for detecting short-range interactions compared to Hi-C (Hsieh et al., 2015, 2016). Indeed, this method successfully detected loops in quiescent cells and in S phase of mitotically dividing yeast (Ohno et al., 2019; Swygert et al., 2019). Here, we use Micro-C on synchronized populations of yeast cells. We observe a robust signal for loops genome-wide. The analysis of this signal generates a model to explain the genomic distribution and frequency of loops and their relationship to cohesin binding to DNA.

RESULTS

Micro-C reveals prevalent chromatin loops in mitotic chromosomes

We reasoned that previous studies failed to observe a robust signal for chromosome loops because they used unsynchronized cells or chromosome capture methods with insufficient resolution (Hsieh et al., 2016; Schalbetter et al., 2017, 2019). With this reasoning, we arrested cells in mitosis, using the inhibitor of microtubule polymerization nocodazole (Nz), in which chromosomes are highly structured and analyzed them by high-resolution Micro-C analysis (Figure1A, Table S1, and (Hsieh et al., 2015, 2016)). In brief, we treated cells with crosslinkers to preserve existing contacts between nucleosomes and then digested the crosslinked chromatin into mono-nucleosomes using the micrococcal nuclease (MNase). The free nucleosomal DNA ends were labeled, ligated, isolated, and subjected to paired-end sequencing. The paired reads from the chimeric sequences gave the coordinates of nucleosomes that were contacting in vivo. We plotted these coordinates producing a contact map of all the interacting nucleosomes in a cell population (Figure 1A), generating a matrix of ~66,000 x 66,000 pixels for the yeast genome.

Three primary 3D features of chromosomes can be found on contact maps. First, local interactions between neighboring nucleosomes are likely, giving rise to a robust signal along the diagonal on the contact map (Figure 1B, unstructured). Second, in a chromatin domain, nucleosomes within the domain will interact with each other more frequently than ones in the neighboring domains, giving rise to a square signal on the contact map (Figure 1B, interaction domain). Third, in a chromatin loop, a pair of distal regions are stably bridged together (5' and 3' loop anchors). The interacting nucleosomes from the loop anchors will generate an off-diagonal spot on the contact map (Figure 1B, loop). Loop length is equal to the length of DNA between the loop anchors and is equal to the distance of the spot from the diagonal.

Micro-C analysis of mitotically arrested cells revealed many off-diagonal spots on the contact map, indicative of the presence of loops. These loops became easily visible when zooming-in on smaller regions of the chromosome with increasing resolution (Figure 1C, top row). The pervasive presence of loops showed on chromosome 7 was observed in the entire genome. These loops were mostly absent in contact maps using datasets from previously published Hi-C maps of mitotic cells (Figure 1C, bottom rows; Figure 1—figure supplement 1A) and Micro-C analysis of asynchronous cells (Figure 1—figure supplement 1B). The improved detection of loops in Micro-C was due to its superior resolution in the range from 100 bp - 30 kb (Figure 1D), as shown in the genome-wide analysis of interaction decaying rate. We used two different loop-calling programs, HiCCUPS and Chromosight, to identify the location of loops genome-wide (Durand et al., 2016; Matthey-Doret et al., 2020). Both identified 10 - 20 times more loops in Micro-C than Hi-C (Table S2 and supplemental file for the complete lists). The total number of 3' and 5' loop anchors was also 10 times greater in Micro-C than Hi-C (Figure 1E). We piled-up the signal from the contact map of a 5 kb region with each loop spot at its center. We compared the center (loop signal) versus the four edges (background) as a ratio and detected a ~4 fold increase in Micro-C, but only ~1.2 fold in Hi-C (Figure 1F). This strong signal for loops allowed us to locate precisely the chromosomal position of the loop anchors genome-wide, and to determine that the average size of loops in yeast was ~8 kilobases. Thus, Micro-C is a robust assay to detect chromosome loops, revealing loops as a principal folding feature of yeast mitotic chromosomes.

Cohesin complex mediates loop formation

We proceeded to identify the protein/s that are responsible to form loops in yeast mitotic chromosomes. In mammals, cohesin is required for loop formation and is present at loop anchors (de Wit et al., 2015). To assess if this was also the case in budding yeast, we first identified the genomic positions of cohesin binding by ChIP-seq of the Mcd1p cohesin subunit (also known as Scc1p/Rad21p) in mitotically arrested cells. Cohesin binds to discrete chromosomal loci termed cohesin associated regions (CARs), which are distributed along chromosomal arms and at

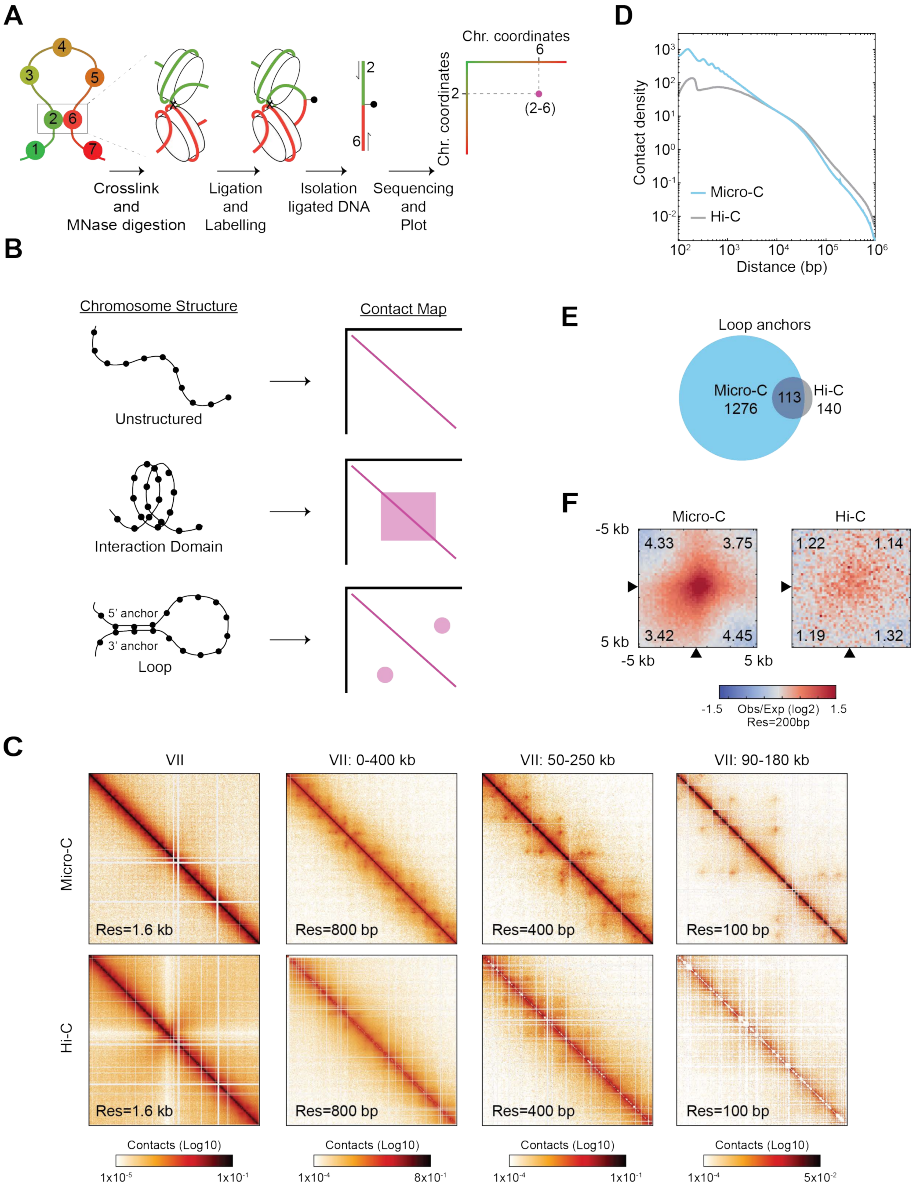

Figure 1. Micro-C reveals prevalent chromatin loops in mitosis.
(A) Micro-C maps chromatin conformation by detecting nucleosomes that interact *in vivo*. Schematic illustrates how two interacting nucleosomes (e.g. 2 and 6) are visualized on the contact map. **(B)** Illustration of different chromosomal structures and their corresponding signal on the contact map. Unstructured chromosomes: only neighboring nucleosomes will be crosslinked producing a linear signal along the diagonal. Interaction Domain: the nucleosomes within a domain will be also crosslinked forming a square along the diagonal. Loop: the nucleosomes at the base of the loop (5' and 3' anchors) will be crosslinked forming a spot away from the diagonal. These different structures can form concomitantly on chromosomes producing contact maps with squares and spots along the diagonal. **(C)** Comparison of contact maps from mitotically arrested cells produced with Micro-C (top) and Hi-C (bottom) (Schalbetter et al., 2019). Contact maps show successive zoom-ins of chromosome VII (from the full 1090 kb to a 90 kb region), across multiple resolutions (from 1.6 kb to 100 bp). All contact maps throughout the manuscript have the standard colormap scheme that uses the shades of red from white (no detectable interactions) to black (maximum interactions detected) in log10 scale. **(D)** Micro-C uncovers chromatin interactions below the kilobase range. Interactions-versus-distance decaying curve shows the normalized contact density (y-axis) against the distance between the pair of crosslinked nucleosomes from 100 bp to 1 Mb (x-axis) for Micro-C and Hi-C (Schalbetter et al., 2019) data. **(E)** Micro-C detects abundant mitotic loops and their corresponding loop anchors. Venn diagrams show how Micro-C identifies 1276 loop anchors that include most of the loop anchors identified by Hi-C. **(F)** Genome-wide average heatmaps show a sharp loop enrichment in Micro-C data. Heatmaps were plotted using the 200 bp resolution data for Micro-C and Hi-C. The plot is a piled-up of the +/- 5 kb region surrounding the loop anchors (black arrows) of every loop identified in Micro-C. Numbers in the corners represent the fold-change of the signal enrichment of the center pixel over the indicated corner pixels (14^2 pixels). The contact map was normalized by matrix balancing and distance, using a diverging colormap with positive signal enrichment in red and negative signals in blue (gradient of normalized contact enrichment is in log2). The fold-change annotation, the color scheme, and the normalization method are used for the piled-up matrix throughout the manuscript unless otherwise mentioned.

centromeres (Blat and Kleckner, 1999; Glynn et al., 2004; Laloraya et al., 2000; Megee and Koshland, 1999). By aligning the Mcd1p ChIP-seq signal with the Micro-C contact map, we observed that the position of every loop anchor overlapped with the position of a CAR (Figure 2A). To evaluate the robustness of this correlation genome-wide, we plotted the Mcd1p ChIP-seq signal of every sequence involved in a loop (the 5' and 3' anchors, and the region in between), by aligning their 5' and 3' anchors (Figure 2B). We observed an enrichment of Mcd1p over >98% of loop anchors. Therefore, loop anchors and cohesin associated regions are highly correlated in mitotic chromosomes of budding yeast.

To gather more information on the portion of the CAR that functions as a loop anchor, we compared the signals from the contact map with the cohesin ChIP-seq. For this analysis, we piled-up the contact map signal of the 5 kilobases regions centered at the intersection of the coordinates of each pair of Mcd1p ChIP-seq peaks (Figure 2C). The portion of the contact map with a contact probability greater than 90%, corresponded to a 1 kilobase region that was centered at the summit of the Mcd1p ChIP-seq peak. Coincidentally, the average width of Mcd1p ChIP-seq peaks is also ~1 kilobase. Thus, loop anchors in budding yeast are centered at the peak of cohesin binding at CARs and both are confined within 1 kilobase region. These results further correlate loop anchors with cohesin associated regions on mitotic chromosomes.

This correlation prompted us to examine the causal role of cohesin in loop formation. To test this possibility, we depleted the cohesin subunit Mcd1p using an auxin-induced degron system (Eng et al., 2014) and analyzed loop formation by Micro-C. Without cohesin, we detected no distinguishable loops by visual inspection of the contact map (Figure 2D and Figure 2—figure supplement 1A). The loops were also gone genome-wide using the loop calling program, dropping from 732 in wild-type cells to just 4 when cohesin was depleted (Figure 2E). Finally, we analyzed the genome-wide averaging signal coming from the piled-up of 5 kilobases regions centered on each loop spot (Figure 2F). The signal for the loop spots was reduced to the background upon Mcd1p depletion. We conclude that cohesin is required for loop formation genome-wide.

Condensin, another member of the SMC family, was known to promote mitotic chromosome structure by condensing chromosomes in vertebrate and yeast cells (Hirano, 2016; Hirano and Mitchison, 1994; Kimura and Hirano, 1997; Saitoh et al., 1994; Strunnikov et al., 1995). We tested whether condensin was also involved in loop formation of mitotic yeast chromosomes by depleting Brn1p, a subunit of condensin. Loop signal was largely unaffected on the contact map (Figure 2—figure supplement 1A), as the number of detected loops modestly decreased from 732 in wild-type to 585 when condensin was depleted (Figure 2—figure supplement 1B). Accordingly, the signal from the averaging analysis of the loop regions was only slightly reduced when condensin was depleted (Figure 2—figure supplement 1C). Contact density decay analysis showed a drop in contacts around the 10 kilobases region (a region corresponding to the size of loops) when cohesin was depleted (Figure 2—figure supplement 1D). This drop was absent when condensin was depleted, corroborating that cohesin, but not condensin was the major driver of loop formation. Furthermore, the number of the inter-chromosomal interactions was similar between wild-type and condensin-depleted cells, unlike cohesin depletion where these interactions doubled. Therefore, cohesin also contributes more to the individualization of chromosomes than condensin (Figure 2—figure supplement 1E and Table S1). In conclusion, cohesin is responsible for the formation of the majority of loops and chromosome individualization in budding yeast mitotic chromosomes, as suggested previously from the modeling of Hi-C studies (Schalbetter et al., 2017).

Cohesin and condensin shape the rDNA locus in mitosis.

The ribosomal DNA locus (RDN) has 75 to 100 tandem repeats of the 9.1 kilobases rDNA unit, with two transcribed loci (RDN37 and RDN5), spaced by two non-transcribed regions (NTS1 and NTS2). In interphase, the RDN locus forms a diffused puff adjacent to the rest of the chromosomal DNA (Guacci et al., 1994). In mitosis, the RDN condenses into a thin line apart from the rest of the genome (Figure 2G) (Guacci et al., 1994). Both cohesin and condensin complexes are needed for RDN condensation (Guacci et al., 1997; Lamothe et al., 2020; Lavoie et al., 2000). However, their impact on chromosomal contacts within the RDN had not been reported.

When we plotted all the contacts in the RDN on one rDNA repeat, we detected a significant difference between interphase and mitosis (Figure 2H, first versus second panel). In interphase where the RDN is a decondensed puff, we detected widespread contacts all over the RDN that were caused by interactions within a repeat and/or between different repeats (intra- or inter-repeats are indistinguishable in sequencing data). While in mitosis where the RDN is a condensed line, the widespread off-diagonal signal was lost. Instead, we observed only the interactions within a repeat and/or between different repeats between the NTS regions where cohesin and condensin bind (Figure 2H and Figure 2—figure supplement 2A) (Guacci et al., 1997; Lamothe et al., 2020; Lavoie et al., 2000). Depletion of cohesin and/or condensin resulted in a contact map pattern that mimicked the wild-type in interphase, reflecting the lack of condensation of these mutants. We also analyzed the total number of contacts between the RDN and the rest of the genome and between the copies of the rDNA. These contacts increased three-fold when cohesin or condensin was depleted from mitotically arrested cells (Figure 2—figure supplement 2B and C). Furthermore, both cohesin and condensin depletion similarly changed the contact decay pattern of the RDN from the wild-type (Figure 2—figure supplement 2D). In the mutants, we observed an increase in long-distance contacts, consistent with the presence of widespread off-diagonal interactions present in those mutants.

These results are consistent with the cytology of the RDN in interphase and mitosis. In interphase, the diffused RDN puff allows for many contacts within the RDN. The shared boundary of the RDN and the rest of the genome promotes contacts between them. In mitosis, the condensation of the RDN to a thin line away

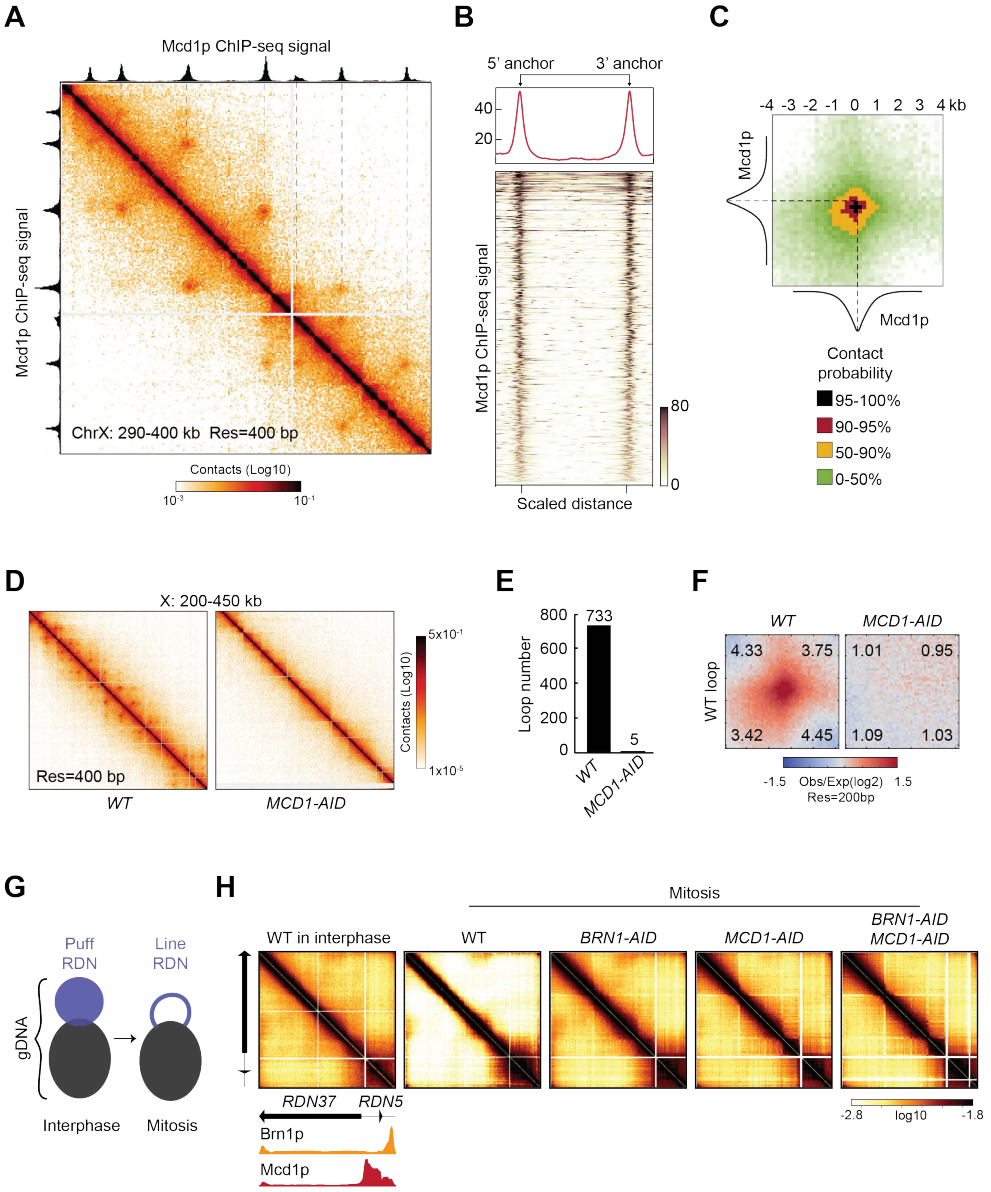

Figure 2. Mitotic loops are cohesin-dependent.
(A) Cohesin peaks colocalize with the loop anchors. Contact map showing the interactions in the 290-400 kb region of chromosome X overlays with Mcd1p ChIP-seq tracks on top and left. The dashed lines indicate the colocalization of loop anchors and Mcd1p peaks. **(B)** Cohesin binding is enriched at loop anchors genome-wide. Heatmap (bottom panel) shows the enrichment of the Mcd1p ChIP-seq signal at the loop anchors genome-wide (732 rows). Pairs of loop anchors were rescaled to the same length. Genome-wide average ChIP-seq signal over the rescaled loop anchors is plotted (top panel). **(C)** Mcd1p peaks center on the loop anchors. Heatmaps were plotted with 200 bp resolution of contact map signal in +/- 4-kb regions surrounding the paired Mcd1p peaks. The contact map is colored by the contact probability with >95% in black, 90-95% in red, 50-90% in yellow, 0-50% in shades of green. The average Mcd1p peak is overlaid with contact maps and centered at the loop bases. **(D)** Loop signal on the contact map is lost upon cohesin depletion. Contact maps for *WT* and *MCD1-AID* Micro-C data show substantial loss of loop signal over chromosome X: 200-450 kb upon Mcd1p degradation. **(E)** Almost no loops are detected upon Mcd1p-depletion. The bar chart shows the loop number called by the HiCCUPS program in *WT* (733) and *MCD1-AID* (5). **(F)** Genome-wide analysis confirms loop signal is gone in *MCD1-AID* cells. Heatmaps were plotted with 200 bp resolution data for *WT* and *MCD1-AID* in +/- 5-kb regions surrounding the wild-type loop anchors. **(G)** Model for RDN structure in interphase and mitosis. RDN (purple) is visualized as a dispersed puff separated from the rest of the genome (black). In mitosis the RDN structures in a thin line. **(H)** Mitotic RDN structure resembles interphase upon cohesin or condensin depletion. Contact maps from one rDNA repeat from wild-type (*WT*) in interphase, followed by mitotically arrested cells in wild-type (*WT*), condensin Brn1p-depleted (*BRN1-AID*), cohesin Mcd1p-depleted (*MCD1-AID*), and cohesin and condensin depleted (*MCD1-AID BRN1-AID)* cells. Standard colormap scheme that uses the shades of red from white (no detectable interactions) to black (maximum interactions detected) in log10 scale. Below the contact map, a model for the genomic organization of the ribosomal DNA repeat (rDNA), where each repeat is made of two transcribed regions (*RDN37* and *RDN5*) and two non-transcribed regions. Below that the ChIP-seq signal of condensin (Brn1p) in yellow and cohesin (Mcd1p) in red on rDNA.

from the rest of the genome limits contacts both between RDN and the rest of the genome, and within the RDN. The ability of condensin and cohesin to restrict local contacts has not been reported previously. The restriction of local interactions could alter the accessibility of gene regulatory regions. This mechanism for cohesin and condensin regulation of gene expression is distinct from their proposed roles as regulators of long-range interactions between enhancers and promoters.

Cohesin organizes chromosomal loops genome-wide.

To better understand how the cohesin rich regions organized the mitotic genome into loops, we performed a more detailed comparison of the cohesin ChIP-seq and the Micro-C contact map. This analysis revealed three features of CARs in loop organizations that were present throughout the yeast genome. First, each CAR formed at least two loops, one by pairing with the CAR that precedes it on the chromosome, and one by pairing with the CAR that follows it (Figure 3A, Loops from adjacent CARs). Thus, each CAR exhibited bidirectional looping. Second, a CAR was also able to pair with CARs that were further down on the chromosome (+2, +3, etc.), resulting in larger loops (Figure 3A, Loops from distal CARs). We defined the looping between distal CARs as loops expansion. Third, loop expansion often stopped at CARs with high Mcd1p ChIP-seq signal consistent with these CARs acting as barriers to loop expansion (Figure 3A, Barriers for loop expansion). Therefore, we made a model that recapitulates how CARs organize the mitotic chromosomes through bidirectional looping, loop expansion, and loop barriers (Figure 3B).

We confirmed and elaborated on these observations through genome-wide analyses. The distribution of the distance between adjacent Mcd1p peaks overlapped with the distribution of the size of the called loops (loops are on average around 8 kb), consistent with most loops being formed between adjacent CARs (Figure 3C). We also analyzed loop expansion by quantifying the percentage of loops being formed by proximal and distal CARs. Eighty-one percent of CARs form loops only with the adjacent CARs, while 19% formed loops with CARs further down the chromosome (Figure 3—figure supplement 1A). This analysis underestimated the number of CARs involved in loop expansion since the loop calling program performed poorly in detecting the spots that were far away from the diagonal (Figure 3—figure supplement 1B). To better estimate the extent of loop expansion and avoid loop calling bias, we piled-up the contact map for regions ranging from +1 to +10 CAR intervals from each loop anchor in the genome. While we detected the loop signal decreased as a function of the distance between the CARs, we observed a strong signal at +2 and +3 CARs (Figure 3D and Figure 3—figure supplement 1C). Moreover, we observed signal up to +5 CARs indicating that loops could be as big as 40 kilobases. We conclude that loop expansion is a common feature of mitotic chromosomes and can occur over large distances.

We noted that the cohesin-rich regions in ChIP-seq presented a wide-range of peak heights. We ordered CARs based on the height of their peaks of cohesin binding from lower to higher, and we defined the top 10% as high-residency CARs. We also noted that the spots on the contact map presented different levels of intensity. We correlated the intensity of a loop in the contact map with the ChIP-seq peak height of the corresponding CAR (Figure 3—figure supplement 1D). We found that high-residency loops correlated with high-residency CARs. We confirmed this correlation comparing the genome-wide averaging signal from loops created by high- and low-intensity CARs (Figure 3E, first versus second panel). Moreover, we performed genome-wide averaging of the signal coming from the pairing of two CARs spaced by a high-residency CAR (Figure 3E, third panel). The signal detected was much weaker when compared to the signal between CARs that did not cross a high-residency CAR, confirming that high-residency CARs block loop expansion. In conclusion, we described how cohesins organize the mitotic chromosomes into loops: each CAR forms a loop with the neighboring CARs in both directions; the looping can spread to CARs further down; CARs with high-residency Mcd1p ChIP-seq signal function as a barrier to loop expansion.

Chromosome loops form during S-phase.

We showed that chromosomes from mitotically arrested cells were organized into loops, but when these loops formed during the cell cycle and how long they persist remained unanswered. To address these questions, we arrested cells in G1. We then released cells from the arrest and monitored loop formation and cohesin binding to chromosomes every 15-minutes for one entire cell cycle. In budding yeast, the Mcd1p subunit of cohesin is synthesized at the beginning of S phase, allowing the assembly of a functional cohesin complex (Guacci et al., 1997; Michaelis et al., 1997). We detected the emergence of loop signal during DNA replication, concomitant with the synthesis and deposition of Mcd1p on chromosomes at CARs (Figure 4A, Figure 4—figure supplement 1A and B, (Ohno et al., 2019)). The signal for loops peaked in G2-M (around 75-minutes) and subsequently disappeared between mitosis and the next cell cycle (Figure 4A, Figure 4—figure supplement 1A and B). The timing of the disappearance of loops corresponded with the loss of Mcd1p and inactivation of cohesin that normally occurs at the onset of anaphase (Figure 4A, Figure 4—figure supplement 1A and B) (Guacci et al., 1997; Michaelis et al., 1997). Furthermore, previous studies in budding yeast showed that loop formation is dependent on cohesin deposition on chromosomes and independent of DNA replication (Dauban et al., 2020; Ohno et al., 2019). These results suggest that the cell cycle control of chromatin loops is achieved by the regulation of functional cohesin. The temporal binding of cohesin to chromosomes during the mammalian cell cycle also correlates with the presence of loops, suggesting a conserved mechanism (Abramo et al., 2019).

The number of loops that were detected at different time intervals was less than the loops detected in mitotically arrested cells. (Figure 4B, Figure 4—figure supplement 1C). The 75-minute sample had the most loops but contained only 50% of the loops observed in mitotically arrested cells. Also, in the 75-minute sample, most of the spots were close to the diagonal as a result of the pairing of adjacent CARs (Figure 4C and D). This inability to detect loop expansion (+2, +3, etc.) was also evident for the other time points (Figure 4—figure supplement 1A). This decreased detection of loops in the time course might reflect increased noise

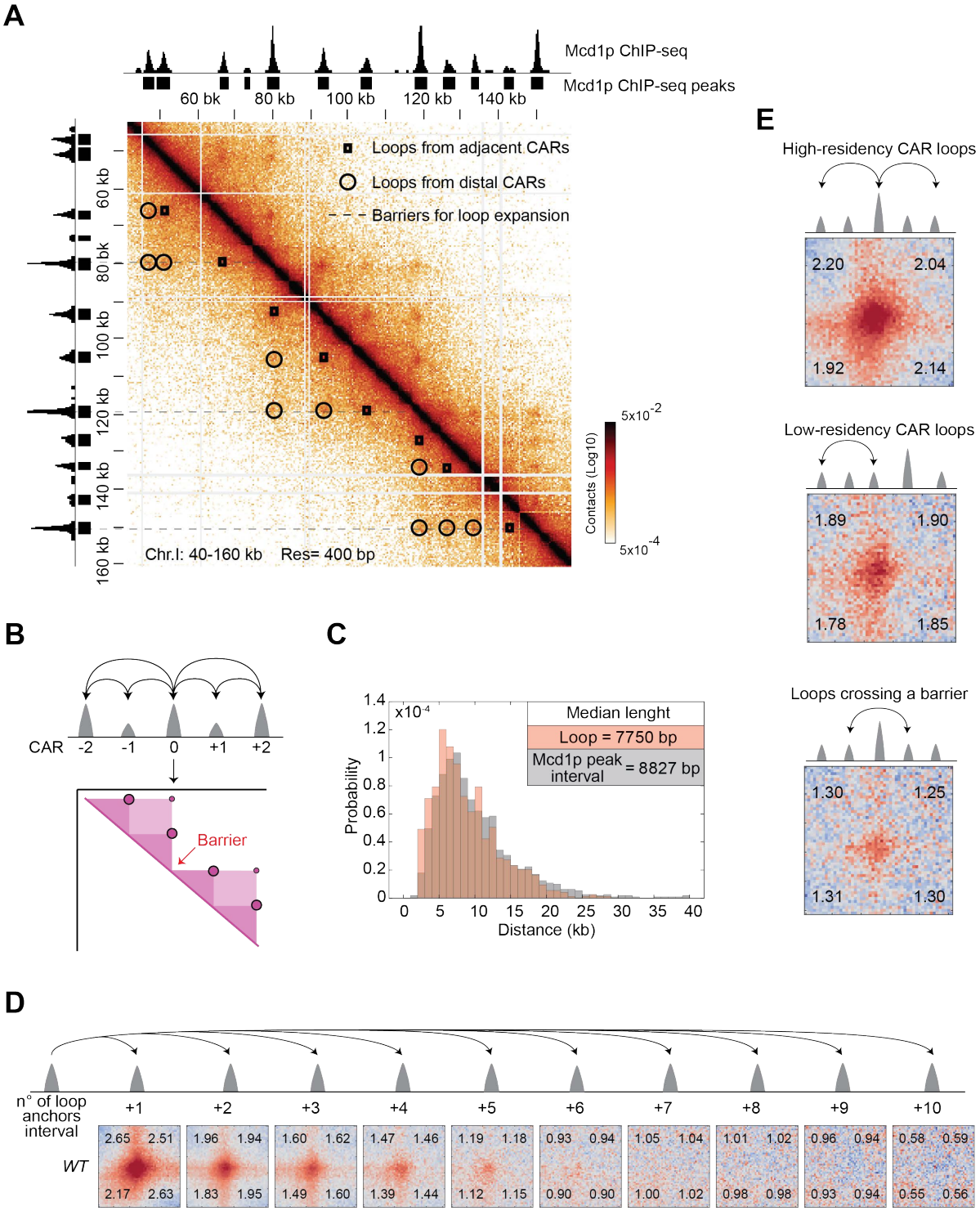

Figure 3. The organization of cohesin-dependent loops.
(A) Features of chromatin loops organization from the contact map. Contact map showing the interaction in the 40-160 kb region of chromosome I overlay with the tracks for Mcd1p ChIP-seq signal and peaks. Squares indicate loops from adjacent CARs. Circles indicate loops from distal CARs. Dashed lines indicate the position of barriers that insulate from loop expansion. **(B)** Model for loops organization. Each CAR (Mcd1p peak) forms a loop with the CAR that follows and a loop with the CAR that precedes. Some CAR can form loops with distal peaks (CAR0 with CAR+2, and CAR0 with CAR-2). The high-residency CAR (peaks with the highest Mcd1p signal) are barriers to loop expansion. **(C)** Loop size is correlated to the cohesin peak interval. The histogram shows the probability of the length distribution for loop size and Mcd1p peak interval in the range from 0 to 40 kb. The inset table highlights the median length. **(D)** Loop signal is detected till the +5 loop anchors interval genome-wide. Heatmaps were plotted with 200 bp resolution data for *WT*. A +/- 5 kb region surrounding each loop anchor and the corresponding loop anchors from +1 to +10 interval. **(E)** The levels of cohesin binding in a loop anchor influence the strength of the corresponding loop and the ability to function as a barrier. Heatmaps were plotted with 200 bp resolution data for *WT*. We plotted a +/- 5 kb region either surrounding the high-residency CARs and the corresponding two-interval CARs (first panel); or surrounding the low-intensity CARs and the corresponding two-interval CARs (second panel); or surrounding a CAR and the corresponding two-interval CAR with a high-residency CAR in the middle (third panel).

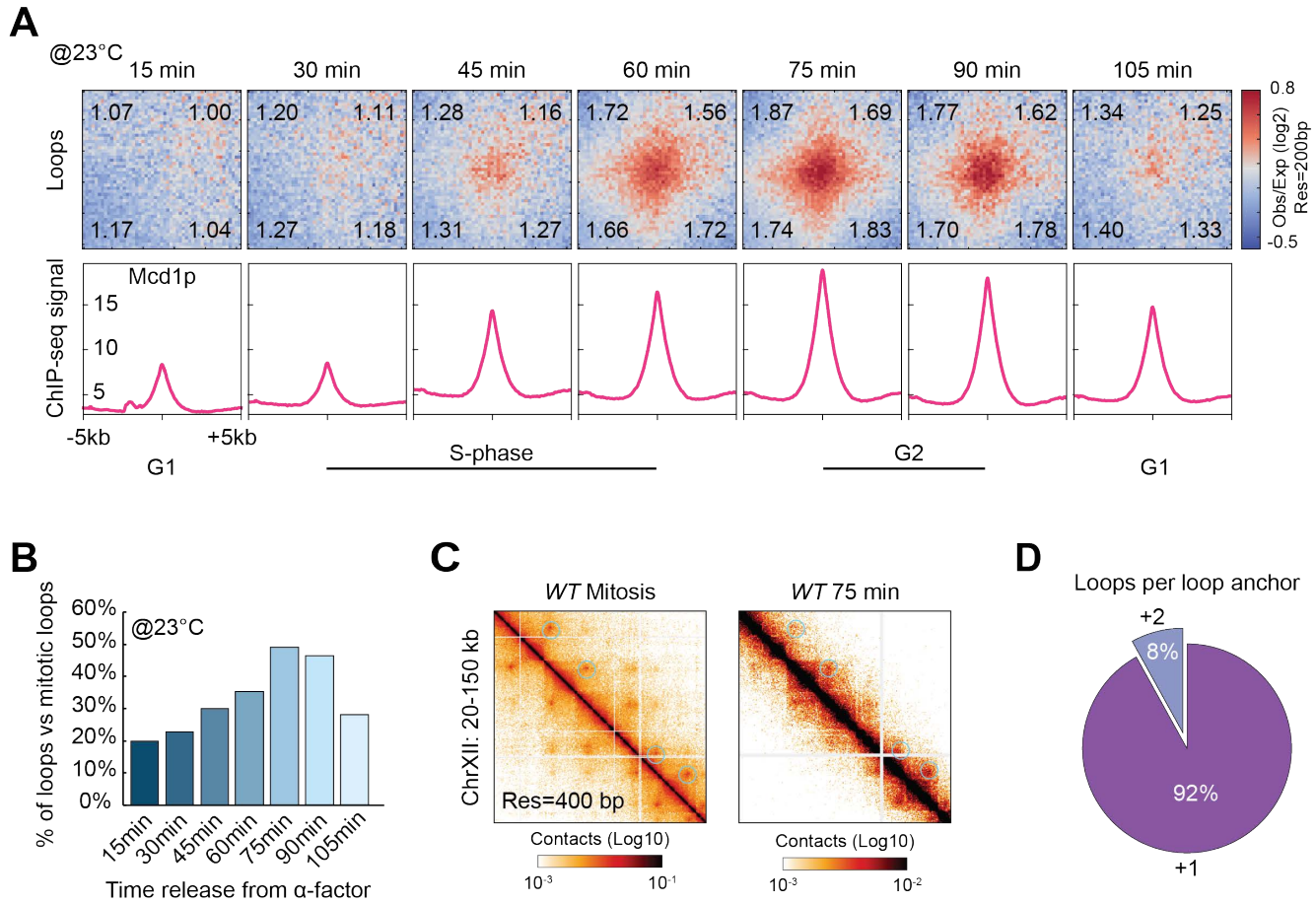

Figure 4. Chromatin loops are cell cycle dependent.
(A) Chromatin loops emerge upon cohesin deposition during DNA replication. The figure shows Micro-C (top) and Mcd1p ChIP-seq (bottom) data across a time course after release from G1 arrest (15 to 105 minutes). Heatmaps were plotted with 200 bp data resolution across a time course in +/- 5-kb regions surrounding the loop anchors identified in the mitotically arrested wild-type data. Average Mcd1p peak intensity was plotted across +/- 5 kb regions around the center of loop anchors at each time point. **(B)** Loop formation peaks in G2 (75-min time point after G1 release). Bar chart represents the percentage of loop numbers at each time point compared to the number of loops found upon mitotic arrest. **(C)** Loops detected during the time course are less defined on the contact map. Snapshots for cells arrested in mitosis (left) and after 75-min release from G1 (right) represent the chromatin interaction in the 20-150 kb region of chromosome XII. Note that snapshot for the 75-min time point is in a higher color contrast for a better loop visualization. **(D)** Only a small subset of loop anchors form loops with distal anchors at the 75-min time point. The pie chart shows the percentage of loop anchors that form loops either with the corresponding neighboring anchors (+1) or with distal anchors (+2) in the 75-min time point.

due to imperfect synchronization. Alternatively, the arrest may stabilize loops. Interestingly, robust chromatin loops were also observed in meiotic yeast cells by Hi-C and in amphibian germinal vesicles by microscopy (Gall and Callan, 1962; Schalbetter et al., 2019).

A key observation from our time course was that most of the cohesin deposition at CARs occurred 15 minutes before the appearance of the majority of loop signal (Figure 4A, compare 45 vs 60 minutes). A model to explain the uncoupling of loop formation and cohesin binding to CARs is that this initial cohesin is not competent for loop extrusion. Loop extrusion is mediated by a different pool of cohesin that is activated later in S phase.

Cohesin regulators affect the size and location of chromosomal loops.

Cohesin has many different activities that are regulated by multiple proteins. Two cohesin regulators, Wpl1p and Pds5p had been previously implicated in regulating chromatin loops in mammals and yeast (Dauban et al., 2020; Haarhuis et al., 2017; Wutz et al., 2017). Wpl1p functions as a negative regulator of cohesin, inhibiting both cohesion and condensation in yeast by removing cohesin from chromosomes (Guacci and Koshland, 2012; Lopez-Serra et al., 2013; Rolef Ben-Shahar et al., 2008). Pds5p binds to cohesin and helps to maintain cohesin binding and cohesion from S-phase until the onset of anaphase (Hartman et al., 2000; Panizza et al., 2000). Pds5p also binds Wpl1p to facilitate the removal of a subset of cohesin (Bloom et al., 2018; Rolef Ben-Shahar et al., 2008). We wondered whether our high-resolution detection of loops might provide new mechanistic insights into the roles of Wlp1p and Pds5p in loop formation.

We depleted Wpl1p from mitotically arrested cells and performed Micro-C to detect loop formation and Mcd1p ChIP-seq to detect cohesin binding on chromosomes. Depletion of Wpl1p reduced the amount of cohesin being detected at CARs (around half of the wild-type) as previously reported for yeast (Rowland et al., 2009; Sutani et al., 2009). It also caused a marked increase in the loops on the contact map (Figure 5A and B, Figure 5—figure supplement 1A and B). Called loops increased from 732 in wild-type to 1588 in cells depleted for Wpl1p, and visual inspection of the contact map showed many more spots linked by distal CARs. Since these loops were often missed by the loop calling program, the increase in the number of loops was likely higher in Wpl1p depleted cells. Therefore, Wpl1p restricts the number of loops and loop expansion in budding yeast as suggested previously from a Hi-C study (Dauban et al., 2020).

The additional loops in Wpl1d-depleted cells appeared to result from the more distal pairing between existing loop anchors in wild-type cells, indicating an increase in loop expansion. Our genome-wide analyses confirmed that the loops present in wild-type were still present in Wpl1p-depleted cells (Figure 5—figure supplement 1C). To assess the loop expansion quantitatively, we quantified how many loops are formed by each loop anchor in one direction. The number of pairing partners for a loop anchor increased in Wlp1-depleted cells compared to wild-type (Figure 5C). We plotted the piled-up all the signals in the contact map for regions ranging from +1 to +10 CAR intervals from each loop anchor in the genome (Figure 5D and Figure 5—figure supplement 1D), to avoid loop calling bias. In Wpl1p-depleted cells, the efficiency of pairing with distal CARs decreased as a function of the distance between the CARs, as observed in wild-type cells. However, two features of this distance dependence changed. First, in wild-type cells, loops with +5 CARs were weak. In contrast, in Wlp1p-depleted cells, the signal from loop anchors +5 was almost as robust as at +2. Second, in wild-type, the signal of loops extended to +5 CARs while in Wlp1p-depleted cells, it extended to +9 CARs (Figure 5D and Figure 5—figure supplement 1D). We conclude that Wpl1p restricts the loop number by decreasing the amount and length of the loop expansion.

We depleted Pds5p from mitotically arrested cells and looked at cohesin binding to chromosomes and loop formation. As published previously, Pds5p depletion caused a marked loss of cohesin all along the chromosome arms (Figure 5E, first column and 5G, first panel) (Guacci et al., 2019). Concomitantly with the loss of cohesin, the loops disappeared from the chromosome arms genome-wide (Figure 5E, first column, 5F and Figure 5—figure supplement 1E). Thus, Pds5p is required for stable cohesin binding and loops on the arms of mitotic chromosomes.

We observed a single peak high-residency peak at the centromeres and a modest reduction of cohesin peaks in the pericentric regions (Figure 5G, second panel). These regions also exhibited an altered loop distribution. The high-residency CAR at the centromere forms loops with the other CARs along the chromosome, generating a prominent stripe pattern that can extend up to hundreds of kilobase (sometimes across an entire chromosome arm) (Figure 5E, second and third panel). This result suggests that in the absence of Pds5p, yeast cohesin can extrude chromatin over long distances, comparable to the size of loops extruded by mammalian cohesin. Thus, Pds5p restricts loop expansion by stabilizing cohesin binding to chromatin.

Chromosome domains in mitosis.

Another structural feature of the contact map was the presence of chromosomal interaction domains. We observed that the high-residency CARs demarcated the chromatin landscape into domains, presumably by blocking loop expansion (Figure 6A). These domains were found all over the chromosomes. We applied the domain-calling algorithm at 1 kilobase resolution to the contact map of wild-type and Mcd1p-depleted cells arrested in mitosis (Figure 6—figure supplement 1A and B). The domains in wild-type cells have boundaries that correlated with high-residency CARs, and we defined those as CAR domains. When cohesin was depleted, we observed different domains that we defined as cohesin-independent domains. To corroborate that the formation of CAR domains was dependent upon cohesin, we piled-up the signal of wild-type and Mcd1p-depleted cells on the rescaled CAR domains, and normalized them to coverage (Figure 6B top) or distance (Figure 6B bottom). We confirmed that the integrity of the CAR domains was dependent on the presence of cohesin. Thus, cohesin promotes domain formation as well as loops in budding yeast.

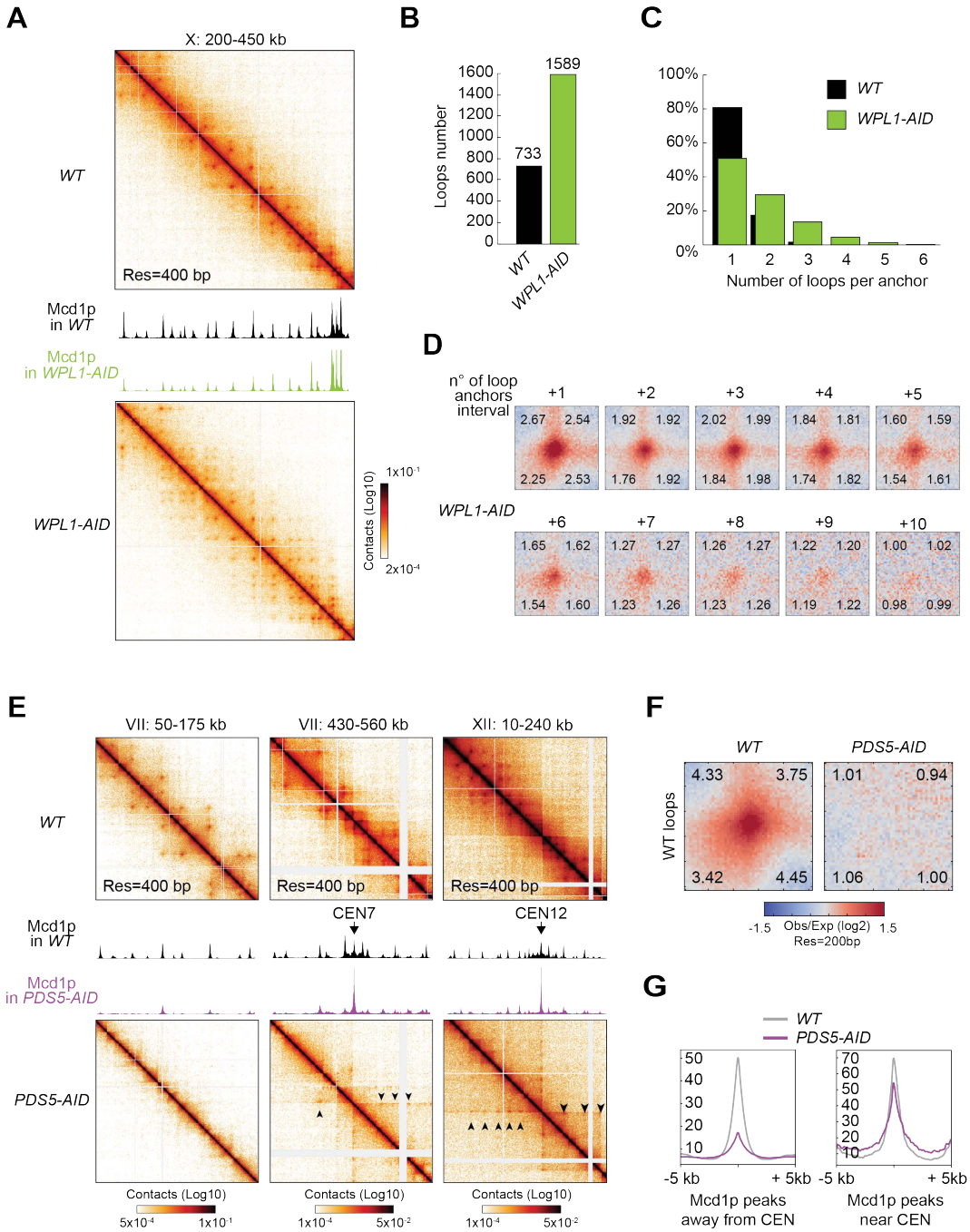

Figure 5. Wpl1p- and Pds5p-depletion perturb the looping pattern.
(A) Wpl1p-depletion causes excessive loop expansion on the contact map. Contact maps for *WT* (top) and *WPL1-AID* (bottom) show the chromatin interactions over the 200-450 kb region of chromosome X. ChIP-seq data for *WT* and *WPL1-AID* are overlaid across the same region. The scale for ChIP-seq is 0-200. **(B)** Wpl1p-depletion doubles the number of loops detected. Bar chart shows the total number of loops called by HiCCUPS in *WT* and *WPL1-AID*. **(C)** Genome-wide analysis confirms loop expansion upon Wpl1p-depletion. Bar chart shows the percentage of the number of loops per anchor for *WPL1-AID* (green) and *WT* (black). **(D)** Wpl1p-depletion results in expansion of the loop signal to further distal loop anchors. Heatmaps were plotted with 200-bp data for *WT* and *WPL1-AID* in +/- 5-kb regions surrounding the wild-type loop anchors and the corresponding loop anchor from a +1 to a +10 interval. **(E)** Pds5p-depletion results in loops between each centromere and surrounding CARs. Contact maps for *WT* (top) and *PDS5-AID* (bottom) shows the chromatin interactions over a chromosome arm on the 50-175 kb region of chromosome VII (left), and centromeric region at 430-560 kb on chromosome VII (middle), or another centromeric region at 10-240 kb of chromosome XII (right). ChIP-seq data for *WT* and *PDS5-AID* are overlaid across the corresponding region in each panel. The scale for ChIP-seq is 0-400. **(F)** Pds5p-depletion results in loss of signal at wild-type loop anchors. Heatmaps were plotted with 200 bp data resolution for *WT* and *PDS5-AID* in +/- 5-kb regions surrounding the wild-type loop anchors. **(G)** Pds5p-depletion causes cohesin depletion from chromosome arms, but not from pericentric regions. Average Mcd1p peak intensity for *WT* and *PDS5-AID* were plotted over +/- 5 kb regions around the peak center. Peaks were sorted into two groups: 1) peaks on the chromosome arms (> 30 kb away from the centromeres) (left); 2) pericentric peaks (< 30-kb away from the centromeres) (right).

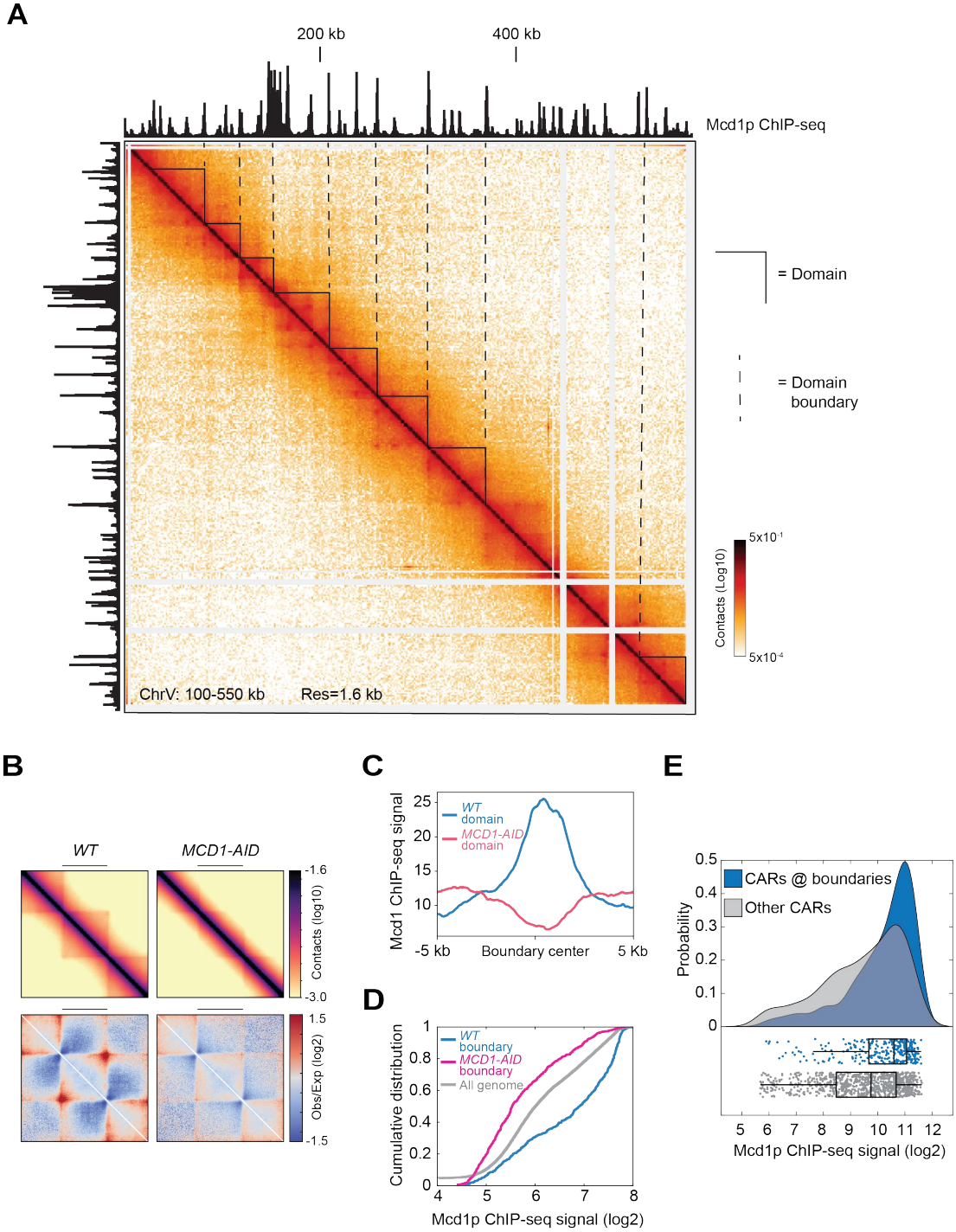

Figure 6. Cohesin depletion alters the domain landscape.
(A) Contact map of mitotic chromatin in wild-type cells reveals the presence of CAR domains and their boundaries. Contact map showing the interaction in the 100-550 kb region of chromosome V overlays with the tracks for Mcd1p ChIP-seq signal. Triangles indicate the CAR domains' position. Dashed lines indicate the position of the CAR domain boundaries. **(B)** The signal at CAR domains is lost upon cohesin depletion. Genome-wide average domain/boundary strength for *WT* (left) and *MCD-AID* (right) are plotted as coverage-normalized contact maps (top) and distance-normalized matrices (bottom) over the CAR domains called in the wild-type. The domains are rescaled to the same length with left and right boundaries aligned on the plot. **(C)** Cohesin is enriched at the boundaries of CAR domains, but not at domains formed upon cohesin depletion. Wild-type Mcd1p ChIP-seq data were plotted separately over +/- 5 kb region around the boundaries of CAR domains in wild-type (blue) or the boundaries present upon Mcd1p-depletion (pink). **(D)** Mcd1p is enriched at CAR domain boundaries and depleted from the domain boundaries present upon cohesin depletion. Cumulative curves are plotted separately as the function of log2 ratio of Mcd1p ChIP-seq signal in the CAR domain boundaries from *WT* (blue), or domain boundaries from *MCD1-AID* (pink), or the entire genome (grey). **(E)** CARs at CAR domain boundaries have higher levels of cohesin binding than other CARs genome-wide. Cumulative curves show the probability distribution of Mcd1p ChIP-seq signal (log2) from CARs present at the CAR boundaries (blue), and from the other CARs (grey). Below the curves are plotted the corresponding Mcd1p ChIP-seq values of each CAR (blue dots for CARs at the CAR boundaries and grey dots for the other CARs). Box and whiskers plot indicates the median values and the quartiles distribution.

To confirm that CARs were at the boundaries of the CAR domains genome-wide, we plotted the cumulative Mcd1p ChIP-seq signal from wild-type cells at CAR domains and cohesin-independent domain boundaries (Figure 6C). A marked enrichment of cohesin was present only at the CAR domain boundaries. Furthermore, cumulative curves for Mcd1p ChIP-seq signal showed that cohesin was enriched at CAR domain boundaries when compared to the rest of the genome (Figure 6D). Conversely, the boundaries of cohesin-independent domains presented a lower cohesin signal when compared to the rest of the genome (Figure 6D). We also observed that the boundaries of CAR domains were enriched at terminators (Figure 6—figure supplement 1C), where CARs are preferentially located. In contrast, the cohesin-independent domain boundaries are mainly localized on promoters. Finally, the CAR domain boundaries presented a stronger Mcd1p ChIP-seq signal when compared to the other CARs genome-wide (Figure 6E), consistent with our finding that high-residency CARs had the capacity to insulate loop expansion to define domains. Our results show that chromosomes are organized into cohesin-dependent (CAR domains) and cohesin-independent domains. The boundaries of the cohesin-dependent domains are determined by CARs with strong cohesin binding. These results are consistent with data from mammalian cells that show the presence of cohesin-dependent and cohesin-independent domains (referred to as compartmental domains). The compartmental domains are thought to be dependent on histones modifications and become more evident upon cohesin depletion (Rao et al., 2017; Schwarzer et al., 2017).

DISCUSSION

In this study, we use Micro-C, a version of chromosome conformation capture with high-resolution to study chromosome architecture in mitotic yeast cells. This approach corroborated several findings from previous Hi-C studies including the presence of cohesin-dependent chromatin loops and the regulation of their size by cohesin regulators Wpl1p and Pds5p. However, our approach generated a robust loop signal on the contact map, where single loops are distinct and easily detectable. We exploited this improved signal to reveal important new features about loop distribution (size and genomic position) and insights into the molecular determinants of loop formation.

One feature of our study is the remarkable correlation between loop anchors and cohesin associated regions (CARs). First, the genomic position of loop anchors correlates almost perfectly with the position of CARs throughout the genome. The pairing of two loop anchors usually occurred between a CAR and the adjacent CAR on either side, but could also partner with more distal CARs (loop expansion). The size of the average loop (~8 Kb) mirrors the average distance between adjacent CARs. Much larger loops were also observed (20-40 Kb), reflecting the distance between distal CARs. These data suggest that CARs determine the size and position of chromatin loops in budding yeast.

The pervasive presence of CARs and their respective loops along the chromosomes suggest that almost all, if not all, regions in the yeast genome can form a loop. Previous studies of chromatin loops in budding yeast estimated that a much smaller fraction of the yeast genome formed loops (Schalbetter et al., 2017, 2019). These studies underestimated the potential looping capacity of the yeast genome based upon the few loops detected by Hi-C. A similar omnipresence of loops is also observed in mammalian cells (Hsieh et al., 2020; Krietenstein et al., 2020; Rao et al., 2014). This shared global distribution suggests an important evolutionarily conserved function for looping chromatin, distinct from the previously proposed function in controlling the expression of a subset of genes. For example, the tethering of sister chromatids by cohesin is already known to promote DNA repair (Sjögren and Nasmyth, 2001; Ström et al., 2004; Unal et al., 2004). Looping by cohesin may contribute to the alignment of homologous repetitive elements between sister chromatids, thereby avoiding unequal sister chromatid exchange. Importantly, budding yeast provides an excellent system to test this and other potentially conserved physiological functions for cohesin-dependent chromatin loops.

Our study also revealed two differences between loop determinants in yeast and mammalian cells. First, in mammals, 85% of loop anchors depend on sites with CTCF and cohesin binding (Rao et al., 2014). In contrast, in yeast cells loops depend on cohesin, since yeast lacks CTCF or any known DNA binding factor that colocalizes with cohesin. Second, in budding yeast, each CAR can form loops with CARs on either side (bidirectional), while in mammals loop formation is often directional correlating with the orientation of convergent CTCF sites (Haarhuis et al., 2017; de Wit et al., 2015; Wutz et al., 2017). The CTCF-independent mechanism in yeast may be a model for loop formation in most other eukaryotes that lack CTCF.

Indeed, from our study of loop anchors, we observed a positive correlation between the level of cohesin binding to a CAR and its probability of acting as a loop anchor in a loop. A key to understanding this correlation comes from two observations. Cohesin binding to chromosomes is split between dynamic and stably bound in yeast and mammals (Gerlich et al., 2006; Hansen et al., 2017). The ChIP-seq peaks at CARs result from stably bound cohesin (half-life >60 minutes (Eng et al., 2014)). The differences in ChIP-seq signal intensity at different CARs likely reflect the fraction of cells in the population with stably bound cohesin at those sites. Second, in our time-course experiment, the ChIP-seq signal from stably bound cohesin precedes the looping by 15 min.

Using these observations, we generated a model to explain the correlation of the level of cohesin binding at CARs with the formation of loops and loop barriers (Figure 7). We suggest that a loop is formed when looping by dynamic cohesin is blocked by the presence of preexisting stably bound cohesin at CARs. For example, dynamic cohesin begins looping between two CARs. If these two CARs have stably bound cohesin in all cells (high-residency CARs), they will always stop the looping at those two CARs, generating a loop between them in all cells. On the other hand, if one of the two CARs has stably bound cohesin in only half the cells, loops will form between those two CARs in only half of the cells. In the other half of the cell population, looping will proceed further and stop at the next CAR occupied by stable

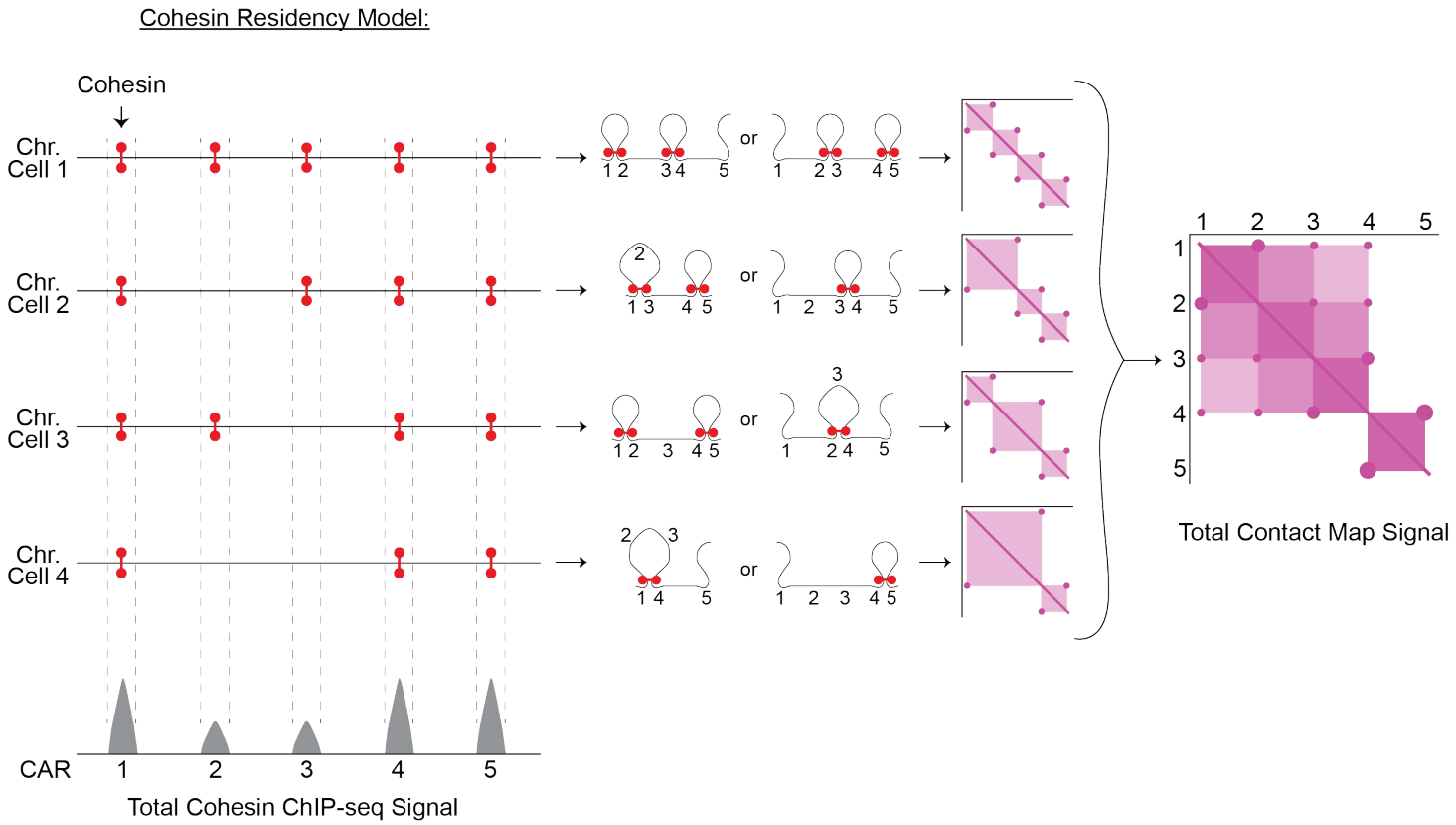

Figure 7. Cohesin residency model for loop formation.
Loop-extrusion with a heterogenous cohesin residency gives rise to an heterogeneous pattern of chromatin looping and domains. The intensity of a cohesin ChIP-seq peak reflects the probability of the CAR being occupied by cohesin in a cell population. ChIP-seq peaks with high signal reflect CARs that are occupied in every cell by cohesin. Low-signal peaks are CARs that are occupied by cohesin only in a fraction of cells. The dynamic population of cohesin with loop extrusion activity will start looping and stop when encountering two cohesin-bound CARs, creating a stable loop. Every loop will result in a spot on the contact map from the stable interaction of the two CARs that function as loop anchors. Furthemore, the sequences inside the loop will have more probability of interacting with each other creating a domain visualized as a square in the contact map. The piled-up of the different squares from individual cells will produce the CAR domain with two high intensity CAR as domain barriers.

cohesin, creating bigger loops (loop expansion). In contrast, a CAR bound by cohesin in every cell always stops dynamic cohesin, blocking the looping that was initiated at neighboring CARs thereby generating a barrier for loop expansion. Therefore, the frequency of a loop between any two CARs is determined in part by the level of stable cohesin binding at those CARs, and by the number of CARs between them. A similar model of stably bound cohesin blocking looping by dynamic cohesin has been suggested from an ingenious approach that allows differentiating contacts within and between sister chromatids (Mitter et al., 2020).

This model can also explain the formation of CAR-domains and its boundaries. The model postulates that loops of different sizes are created among the CARs between two high-residency CARs in different cells. The sequences within each loop will interact with each other preferentially creating a small 'loop domain'. The 'loop domains' of different sizes from individual cells will be piled-up in the contact map, resulting in the observed CAR domain (Figure 7, right side). The high-residency CAR will block the loop extrusion activity and function as a barrier for the CAR domain. A similar model for loop extrusion and formation of domains was also postulated for mammalian cells (Fudenberg et al., 2016).

The generation of this model was also driven by our detailed characterization of the loop expansion in Wlp1p- and Pds5p-depleted cells. Pds5p helps cohesin to establish cohesion but also forms a complex with Wlp1p to remove cohesin from chromosomes. It has been proposed that depletion of Wlp1p or Pds5p stabilizes the binding of dynamic cohesin, increasing the processivity of its looping activity and loop size (Haarhuis et al., 2017). However, this hypothesis alone could not explain additional differences between loop expansion and location in Wpl1p- and Pds5p-depletion revealed in this study.

In Wlp1p-depleted cells, the number of loops and loop expansion increased genome-wide compared to wild type. We can explain these changes in looping through our cohesin occupancy model and the fact that in budding yeast Wpl1p depletion reduced cohesin binding at CARs about 50% genome-wide (this study, (Guacci et al., 2019; Rowland et al., 2009; Sutani et al., 2009) This reduced binding of cohesin is not well understood but might reflect a role for Wlp1p in removing the non-specific binding of cohesin genome-wide to allow its accumulation at CARs (Bloom et al., 2018). We suggest that this defect in cohesin loading decreases the number of CARs that are occupied by cohesin in the cell population. As a result, in these cells dynamic cohesin can pair with more distal CARs, allowing more loop formation and expansion.

In Pds5-depleted cells, the number of loops decreased and more pronounced loop expansion (100's of kilobases) occurred only from the centromere compared to wild-type or Wlp1p-depleted cells. These differences can also be explained by our occupancy model and the dramatic differences in cohesin binding to different CARs in Pds5p-depleted cells. In ChIP-seq we observed a prominent cohesin binding at the centromeres, greatly reduced binding in the centromere-proximal regions, and almost no binding at centromere-distal regions. We suggest that the high occupancy of cohesin at the centromere will always stop the looping of the dynamic cohesin. On the other side, the looping will proceed down the arm for long distances before being stopped by the occasional CAR site occupied by stably bound cohesin. This process will result in a series of loops emanating from the centromeres to the arms in a cross pattern, as observed in our contact map. The low occupancy of the other CARs with stable cohesin is so low that dynamic cohesin is stopped rarely between these CARs, and therefore rarely generates loops on chromosome arms. Thus the two very different looping patterns of Wpl1p- and Pds5p-depletion can be explained by our occupancy model.

In summary, our model suggests that loop expansion is restrained not only by decreasing the level of dynamic cohesin with looping activity, but also by increasing the level of stably bound cohesin to CARs. In mammalian cells looping by dynamic cohesin may also be blocked by cohesin that is stably bound to chromosomes because of Sororin or CTCF.

REFERENCES

Abramo, K., Valton, A.-L., Venev, S.V., Ozadam, H., Fox, A.N., and Dekker, J. (2019). A chromosome folding intermediate at the condensin-to-cohesin transition during telophase. Nat. Cell Biol. 21, 1393–1402.

Blat, Y., and Kleckner, N. (1999). Cohesins bind to preferential sites along yeast chromosome III, with differential regulation along arms versus the centric region. Cell 98, 249–259.

Bloom, M.S., Koshland, D., and Guacci, V. (2018). Cohesin Function in Cohesion, Condensation, and DNA Repair Is Regulated by Wpl1p via a Common Mechanism in Saccharomyces cerevisiae. Genetics 208, 111–124.

Dauban, L., Montagne, R., Thierry, A., Lazar-Stefanita, L., Bastié, N., Gadal, O., Cournac, A., Koszul, R., and Beckouët, F. (2020). Regulation of Cohesin-Mediated Chromosome Folding by Eco1 and Other Partners. Mol. Cell.

Davidson, I.F., Bauer, B., Goetz, D., Tang, W., Wutz, G., and Peters, J.-M. (2019). DNA loop extrusion by human cohesin. Science 366, eaaz3418–1345.

Dekker, J., Rippe, K., Dekker, M., and Kleckner, N. (2002). Capturing chromosome conformation. Science 295, 1306–1311.

Deng, W., Lee, J., Wang, H., Miller, J., Reik, A., Gregory, P.D., Dean, A., and Blobel, G.A. (2012). Controlling long-range genomic interactions at a native locus by targeted tethering of a looping factor. Cell 149, 1233–1244.

Denker, A., and de Laat, W. (2016). The second decade of 3C technologies: detailed insights into nuclear organization. Genes Dev. 30, 1357–1382.

Dixon, J.R., Selvaraj, S., Yue, F., Kim, A., Li, Y., Shen, Y., Hu, M., Liu, J.S., and Ren, B. (2012). Topological domains in mammalian genomes identified by analysis of chromatin interactions. Nature 485, 376–380.

Durand, N.C., Shamim, M.S., Machol, I., Rao, S.S.P., Huntley, M.H., Lander, E.S., and Aiden, E.L. (2016). Juicer Provides a

One-Click System for Analyzing Loop-Resolution Hi-C Experiments. Cell Syst 3, 95–98.

Eng, T., Guacci, V., and Koshland, D. (2014). ROCC, a conserved region in cohesin's Mcd1 subunit, is essential for the proper regulation of the maintenance of cohesion and establishment of condensation. Mol. Biol. Cell 25, 2351–2364.

Fudenberg, G., Imakaev, M., Lu, C., Goloborodko, A., Abdennur, N., and Mirny, L.A. (2016). Formation of Chromosomal Domains by Loop Extrusion. Cell Rep. 15, 2038–2049.

Gall, J.G., and Callan, H.G. (1962). H3 uridine incorporation in lampbrush chromosomes. Proc. Natl. Acad. Sci. U. S. A. 48, 562–570.

Ganji, M., Shaltiel, I.A., Bisht, S., Kim, E., Kalichava, A., Haering, C.H., and Dekker, C. (2018). Real-time imaging of DNA loop extrusion by condensin. Science 360, 102–105.

Gerlich, D., Koch, B., Dupeux, F., Peters, J.-M., and Ellenberg, J. (2006). Live-cell imaging reveals a stable cohesin-chromatin interaction after but not before DNA replication. Curr. Biol. 16, 1571–1578.

Glynn, E.F., Megee, P.C., Yu, H.-G., Mistrot, C., Unal, E., Koshland, D.E., DeRisi, J.L., and Gerton, J.L. (2004). Genome-wide mapping of the cohesin complex in the yeast Saccharomyces cerevisiae. PLoS Biol. 2, E259.

Guacci, V., and Koshland, D. (2012). Cohesin-independent segregation of sister chromatids in budding yeast. Mol. Biol. Cell 23, 729–739.

Guacci, V., Hogan, E., and Koshland, D. (1994). Chromosome condensation and sister chromatid pairing in budding yeast. J. Cell Biol. 125, 517–530.

Guacci, V., Koshland, D., and Strunnikov, A. (1997). A direct link between sister chromatid cohesion and chromosome condensation revealed through the analysis of MCD1 in S. cerevisiae. Cell 91, 47–57.

Guacci, V., Chatterjee, F., Robison, B., and Koshland, D.E. (2019). Communication between distinct subunit interfaces of the cohesin complex promotes its topological entrapment of DNA. Elife 8.

Guo, Y., Xu, Q., Canzio, D., Shou, J., Li, J., Gorkin, D.U., Jung, I., Wu, H., Zhai, Y., Tang, Y., et al. (2015). CRISPR Inversion of CTCF Sites Alters Genome Topology and Enhancer/Promoter Function. Cell 162, 900–910.

Haarhuis, J.H.I., van der Weide, R.H., Blomen, V.A., Yáñez-Cuna, J.O., Amendola, M., van Ruiten, M.S., Krijger, P.H.L., Teunissen, H., Medema, R.H., van Steensel, B., et al. (2017). The Cohesin Release Factor WAPL Restricts Chromatin Loop Extension. Cell 169, 693–707.e14.

Hadjur, S., Williams, L.M., Ryan, N.K., Cobb, B.S., Sexton, T., Fraser, P., Fisher, A.G., and Merkenschlager, M. (2009). Cohesins form chromosomal cis-interactions at the developmentally regulated IFNG locus. Nature 460, 410–413.

Handoko, L., Xu, H., Li, G., Ngan, C.Y., Chew, E., Schnapp, M., Lee, C.W.H., Ye, C., Ping, J.L.H., Mulawadi, F., et al. (2011). CTCF-mediated functional chromatin interactome in pluripotent cells. Nat. Genet. 43, 630–638.

Hansen, A.S., Pustova, I., Cattoglio, C., Tjian, R., and Darzacq, X. (2017). CTCF and cohesin regulate chromatin loop stability with distinct dynamics. Elife 6, e25776.

Hartman, T., Stead, K., Koshland, D., and Guacci, V. (2000). Pds5p is an essential chromosomal protein required for both sister chromatid cohesion and condensation in Saccharomyces cerevisiae. J. Cell Biol. 151, 613–626.

Hassler, M., Shaltiel, I.A., and Haering, C.H. (2018). Towards a Unified Model of SMC Complex Function. Curr. Biol. 28, R1266–R1281.

Heger, P., Marin, B., Bartkuhn, M., Schierenberg, E., and Wiehe, T. (2012). The chromatin insulator CTCF and the emergence of metazoan diversity. Proc. Natl. Acad. Sci. U. S. A. 109, 17507–17512.

Hirano, T. (2016). Condensin-Based Chromosome Organization from Bacteria to Vertebrates. Cell 164, 847–857.

Hirano, T., and Mitchison, T.J. (1994). A heterodimeric coiled-coil protein required for mitotic chromosome condensation in vitro. Cell 79, 449–458.

Hsieh, T.-H.S., Weiner, A., Lajoie, B., Dekker, J., Friedman, N., and Rando, O.J. (2015). Mapping Nucleosome Resolution Chromosome Folding in Yeast by Micro-C. Cell 162, 108–119.

Hsieh, T.-H.S., Fudenberg, G., Goloborodko, A., and Rando, O.J. (2016). Micro-C XL: assaying chromosome conformation from the nucleosome to the entire genome. Nat. Methods 13, 1009–1011.

Hsieh, T.-H.S., Cattoglio, C., Slobodyanyuk, E., Hansen, A.S., Rando, O.J., Tjian, R., and Darzacq, X. (2020). Resolving the 3D Landscape of Transcription-Linked Mammalian Chromatin Folding. Mol. Cell 78, 539–553.e8.

Kempfer, R., and Pombo, A. (2020). Methods for mapping 3D chromosome architecture. Nat. Rev. Genet. 21, 207–226.

Kim, Y., Shi, Z., Zhang, H., Finkelstein, I.J., and Yu, H. (2019). Human cohesin compacts DNA by loop extrusion. - PubMed - NCBI. Science 47, eaaz4475–1349.

Kimura, K., and Hirano, T. (1997). ATP-dependent positive supercoiling of DNA by 13S condensin: a biochemical implication for chromosome condensation. Cell 90, 625–634.

Krietenstein, N., Abraham, S., Venev, S.V., Abdennur, N., Gibcus, J., Hsieh, T.-H.S., Parsi, K.M., Yang, L., Maehr, R., Mirny, L.A., et al. (2020). Ultrastructural Details of Mammalian Chromosome Architecture. Mol. Cell 78, 554–565.e7.

Laloraya, S., Guacci, V., and Koshland, D. (2000). Chromosomal addresses of the cohesin component Mcd1p. J. Cell Biol. 151, 1047–1056.

Lamothe, R., Costantino, L., and Koshland, D.E. (2020). The spatial regulation of condensin activity in chromosome condensation. Genes Dev.

Lavoie, B.D., Tuffo, K.M., Oh, S., Koshland, D., and Holm, C. (2000). Mitotic chromosome condensation requires Brn1p, the yeast homologue of Barren. Mol. Biol. Cell 11, 1293–1304.

Li, G., Ruan, X., Auerbach, R.K., Sandhu, K.S., Zheng, M., Wang, P., Poh, H.M., Goh, Y., Lim, J., Zhang, J., et al. (2012). Extensive promoter-centered chromatin interactions provide a topological basis for transcription regulation. Cell 148, 84–98.

Li, Y., Haarhuis, J.H.I., Cacciatore, Á.S., Oldenkamp, R., van Ruiten, M.S., Willems, L., Teunissen, H., Muir, K.W., de Wit, E., Rowland, B.D., et al. (2020). The structural basis for cohesin-CTCF-anchored loops. Nature 1–9.

Lieberman-Aiden, E., van Berkum, N.L., Williams, L., Imakaev, M., Ragoczy, T., Telling, A., Amit, I., Lajoie, B.R., Sabo, P.J., Dorschner, M.O., et al. (2009). Comprehensive mapping of long-range interactions reveals folding principles of the human genome. Science 326, 289–293.

Lopez-Serra, L., Lengronne, A., Borges, V., Kelly, G., and Uhlmann, F. (2013). Budding yeast Wapl controls sister chromatid cohesion maintenance and chromosome condensation. Curr. Biol. 23, 64–69.

Marsden, M.P., and Laemmli, U.K. (1979). Metaphase chromosome structure: evidence for a radial loop model. Cell 17, 849–858.

Matthey-Doret, C., Baudry, L., Breuer, A., Montagne, R., Guiglielmoni, N., Scolari, V., Jean, E., Campeas, A., Chanut, P.-H., Oriol, E., et al. (2020). Chromosight: A computer vision program for pattern detection in chromosome contact maps.

Megee, P.C., and Koshland, D. (1999). A functional assay for centromere-associated sister chromatid cohesion. Science 285, 254–257.

Michaelis, C., Ciosk, R., and Nasmyth, K. (1997). Cohesins: chromosomal proteins that prevent premature separation of sister chromatids. Cell 91, 35–45.

Mitter, M., Gasser, C., Takacs, Z., Langer, C.C.H., Tang, W., Jessberger, G., Beales, C.T., Neuner, E., Ameres, S.L., Peters, J.-M., et al. (2020). Sister-chromatid-sensitive Hi-C reveals the conformation of replicated human chromosomes.

Nora, E.P., Lajoie, B.R., Schulz, E.G., Giorgetti, L., Okamoto, I., Servant, N., Piolot, T., van Berkum, N.L., Meisig, J., Sedat, J., et al. (2012). Spatial partitioning of the regulatory landscape of the X-inactivation centre. Nature 485, 381–385.

Nora, E.P., Goloborodko, A., Valton, A.-L., Gibcus, J.H., Uebersohn, A., Abdennur, N., Dekker, J., Mirny, L.A., and Bruneau, B.G. (2017). Targeted Degradation of CTCF Decouples Local Insulation of Chromosome Domains from Genomic Compartmentalization. Cell 169, 930–944.e22.

Ohno, M., Ando, T., Priest, D.G., Kumar, V., Yoshida, Y., and Taniguchi, Y. (2019). Sub-nucleosomal Genome Structure Reveals Distinct Nucleosome Folding Motifs. Cell 176, 520–534.e25.

Onn, I., Heidinger-Pauli, J.M., Guacci, V., Unal, E., and Koshland, D.E. (2008). Sister chromatid cohesion: a simple concept with a complex reality. Annu. Rev. Cell Dev. Biol. 24, 105–129.

Palstra, R.-J., Tolhuis, B., Splinter, E., Nijmeijer, R., Grosveld, F., and de Laat, W. (2003). The beta-globin nuclear compartment in development and erythroid differentiation. Nat. Genet. 35, 190–194.

Panizza, S., Tanaka, T., Hochwagen, A., Eisenhaber, F., and Nasmyth, K. (2000). Pds5 cooperates with cohesin in maintaining sister chromatid cohesion. Curr. Biol. 10, 1557–1564.

Parelho, V., Hadjur, S., Spivakov, M., Leleu, M., Sauer, S., Gregson, H.C., Jarmuz, A., Canzonetta, C., Webster, Z., Nesterova, T., et al. (2008). Cohesins functionally associate with CTCF on mammalian chromosome arms. Cell 132, 422–433.

Paulson, J.R., and Laemmli, U.K. (1977). The structure of histone-depleted metaphase chromosomes. Cell 12, 817–828.

Rao, S.S.P., Huntley, M.H., Durand, N.C., Stamenova, E.K., Bochkov, I.D., Robinson, J.T., Sanborn, A.L., Machol, I., Omer, A.D., Lander, E.S., et al. (2014). A 3D map of the human genome at kilobase resolution reveals principles of chromatin looping. - PubMed - NCBI. Cell 159, 1665–1680.

Rao, S.S.P., Huang, S.-C., Glenn St Hilaire, B., Engreitz, J.M., Perez, E.M., Kieffer-Kwon, K.-R., Sanborn, A.L., Johnstone, S.E., Bascom, G.D., Bochkov, I.D., et al. (2017). Cohesin Loss Eliminates All Loop Domains. Cell 171, 305–320.e24.

Rolef Ben-Shahar, T., Heeger, S., Lehane, C., East, P., Flynn, H., Skehel, M., and Uhlmann, F. (2008). Eco1-dependent cohesin acetylation during establishment of sister chromatid cohesion. Science 321, 563–566.

Rowland, B.D., Roig, M.B., Nishino, T., Kurze, A., Uluocak, P., Mishra, A., Beckouët, F., Underwood, P., Metson, J., Imre, R., et al. (2009). Building sister chromatid cohesion: smc3 acetylation counteracts an antiestablishment activity. Mol. Cell 33, 763–774.

Rowley, M.J., Poulet, A., Nichols, M.H., Bixler, B.J., Sanborn, A.L., Brouhard, E.A., Hermetz, K., Linsenbaum, H., Csankovszki, G., Lieberman Aiden, E., et al. (2020). Analysis of Hi-C data using SIP effectively identifies loops in organisms from C. elegans to mammals. Genome Res. 30, 447–458.

Saitoh, N., Goldberg, I.G., Wood, E.R., and Earnshaw, W.C. (1994). ScII: an abundant chromosome scaffold protein is a member of a family of putative ATPases with an unusual predicted tertiary structure. J. Cell Biol. 127, 303–318.

Sanborn, A.L., Rao, S.S.P., Huang, S.-C., Durand, N.C., Huntley, M.H., Jewett, A.I., Bochkov, I.D., Chinnappan, D., Cutkosky, A., Li, J., et al. (2015). Chromatin extrusion explains key features of loop and domain formation in wild-type and engineered genomes. Proc. Natl. Acad. Sci. U. S. A. 112, E6456–E6465.

Schalbetter, S.A., Goloborodko, A., Fudenberg, G., Belton, J.-M., Miles, C., Yu, M., Dekker, J., Mirny, L., and Baxter, J. (2017). SMC complexes differentially compact mitotic chromosomes according to genomic context. Nat. Cell Biol. 19, 1071–1080.

Schalbetter, S.A., Fudenberg, G., Baxter, J., Pollard, K.S., and Neale, M.J. (2019). Principles of meiotic chromosome assembly revealed in S. cerevisiae. Nat. Commun. 10, 4795–4712.

Schoenfelder, S., and Fraser, P. (2019). Long-range enhancer-promoter contacts in gene expression control. Nat. Rev. Genet. 20, 437–455.

Schwarzer, W., Abdennur, N., Goloborodko, A., Pekowska, A., Fudenberg, G., Loe-Mie, Y., Fonseca, N.A., Huber, W., Haering, C.H., Mirny, L., et al. (2017). Two independent modes of chromatin organization revealed by cohesin removal. Nature 551, 51–56.

Sexton, T., Yaffe, E., Kenigsberg, E., Bantignies, F., Leblanc, B., Hoichman, M., Parrinello, H., Tanay, A., and Cavalli, G. (2012). Three-dimensional folding and functional organization principles of the Drosophila genome. Cell 148, 458–472.

Sjögren, C., and Nasmyth, K. (2001). Sister chromatid cohesion is required for postreplicative double-strand break repair in Saccharomyces cerevisiae. Curr. Biol. 11, 991–995.

Splinter, E., Heath, H., Kooren, J., Palstra, R.-J., Klous, P., Grosveld, F., Galjart, N., and de Laat, W. (2006). CTCF mediates long-range chromatin looping and local histone modification in the beta-globin locus. Genes Dev. 20, 2349–2354.

Ström, L., Lindroos, H.B., Shirahige, K., and Sjögren, C. (2004). Postreplicative recruitment of cohesin to double-strand breaks is required for DNA repair. Mol. Cell 16, 1003–1015.

Strunnikov, A.V., Hogan, E., and Koshland, D. (1995). SMC2, a Saccharomyces cerevisiae gene essential for chromosome segregation and condensation, defines a subgroup within the SMC family. Genes Dev. 9, 587–599.

Sutani, T., Kawaguchi, T., Kanno, R., Itoh, T., and Shirahige, K. (2009). Budding yeast Wpl1(Rad61)-Pds5 complex counteracts sister chromatid cohesion-establishing reaction. Curr. Biol. 19, 492–497.

Swygert, S.G., Kim, S., Wu, X., Fu, T., Hsieh, T.-H., Rando, O.J., Eisenman, R.N., Shendure, J., McKnight, J.N., and Tsukiyama, T. (2019). Condensin-Dependent Chromatin Compaction Represses Transcription Globally during Quiescence. Mol. Cell 73, 533–546.e4.

Tolhuis, B., Palstra, R.J., Splinter, E., Grosveld, F., and de Laat, W. (2002). Looping and interaction between hypersensitive sites in the active beta-globin locus. Mol. Cell 10, 1453–1465.

Unal, E., Arbel-Eden, A., Sattler, U., Shroff, R., Lichten, M., Haber, J.E., and Koshland, D. (2004). DNA damage response pathway uses histone modification to assemble a double-strand break-specific cohesin domain. Mol. Cell 16, 991–1002.

Wang, X., Brandão, H.B., Le, T.B.K., Laub, M.T., and Rudner, D.Z. (2017). Bacillus subtilis SMC complexes juxtapose chromosome arms as they travel from origin to terminus. - PubMed - NCBI. Science 355, 524–527.

Wendt, K.S., Yoshida, K., Itoh, T., Bando, M., Koch, B., Schirghuber, E., Tsutsumi, S., Nagae, G., Ishihara, K., Mishiro, T., et al. (2008). Cohesin mediates transcriptional insulation by CCCTC-binding factor. Nature 451, 796–801.

de Wit, E., Vos, E.S.M., Holwerda, S.J.B., Valdes-Quezada, C., Verstegen, M.J.A.M., Teunissen, H., Splinter, E., Wijchers, P.J., Krijger, P.H.L., and de Laat, W. (2015). CTCF Binding Polarity Determines Chromatin Looping. Mol. Cell 60, 676–684.

Wutz, G., Várnai, C., Nagasaka, K., Cisneros, D.A., Stocsits, R.R., Tang, W., Schoenfelder, S., Jessberger, G., Muhar, M., Hossain, M.J., et al. (2017). Topologically associating domains and chromatin loops depend on cohesin and are regulated by CTCF, WAPL, and PDS5 proteins. EMBO J. 36, 3573–3599.

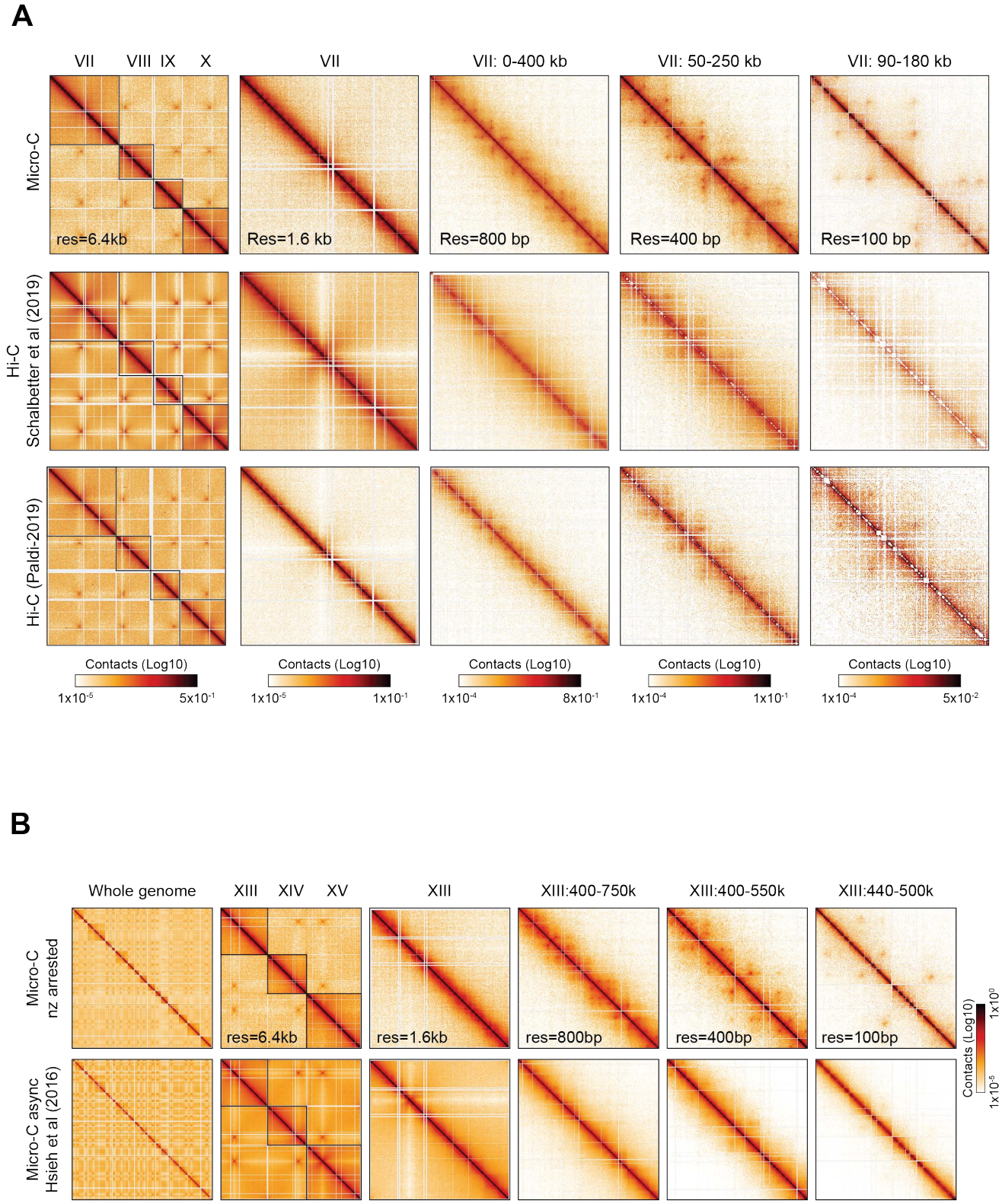

Figure 1—figure supplement 1. Comparison of Micro-C and Hi-C mapping in budding yeast.
(A) Micro-C in mitotically arrested cells detects more loops than Hi-C. Comparison of contact maps from mitotically arrested cells produced with Micro-C (top), Hi-C (center) (Schalbetter et al., 2019), and Hi-C (bottom) (Paldi et al., 2020). Contact maps show contacts between chromosomes VII to X at 6.4 kb resolution (first column). Contact maps show successive zoom-ins of chromosome VII (from the full 1090 kb to a 90 kb region), across multiple resolutions (from 1.6 kb to 100 bp). Standard colormap scheme that uses the shades of red from white (no detectable interactions) to black (maximum interactions detected) in log10 scale. **(B)** Micro-C detects loops in mitotically arrested, but not in asynchronous cells. Comparison of contact maps from mitotically arrested cells with Micro-C (top), and unsynchronized cell with Micro-C (bottom) (Hsieh et al. 2016), Contact maps show contacts between the whole genome (first column), followed by contacts from chromosomes XII to XV at 6.4 kb resolution (second column). Following contact maps show successive zoom-ins of chromosome XII (from the full 924 kb to a 60 kb region), across multiple resolutions (from 1.6 kb to 100 bp). Standard colormap scheme that uses the shades of red from white (no detectable interactions) to black (maximum interactions detected) in log10 scale.

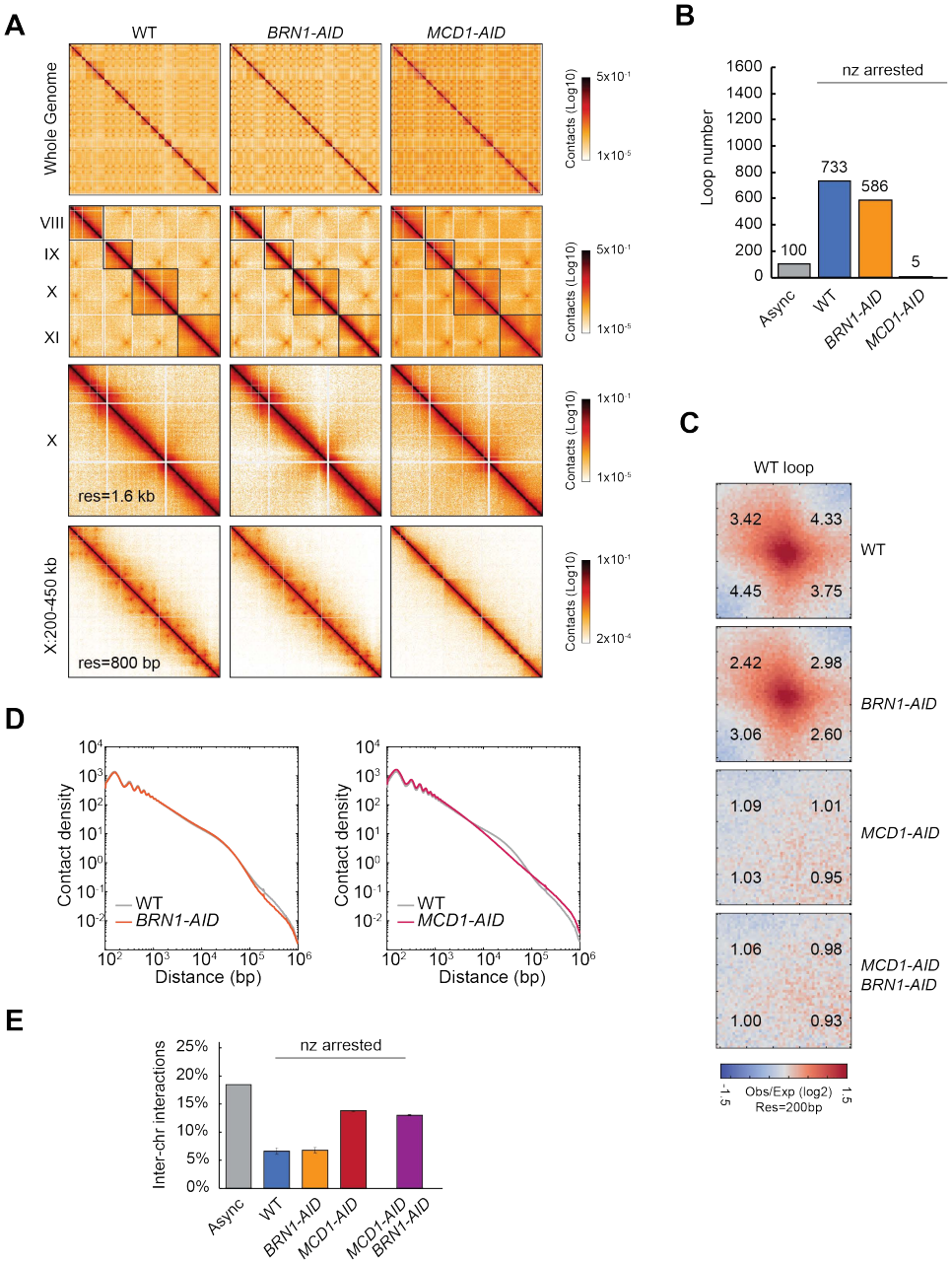

Figure 2—figure supplement 1. Mitotic loops are cohesin-dependent.
(A) The majority of the loops are cohesin-dependent. Contact maps from mitotically arrested cells produced with Micro-C on wild-type (*WT*), cohesin Mcd1p-depleted (*MCD1-AID*), and condensin Brn1p-depleted (*BRN1-AID*) cells. Contact maps show contacts between the whole genome (first row), followed by contacts from chromosomes VIII to XI at 6.4 kb resolution (second row). Following contact maps show chromosome X and a zoomed-in region (from the full 745 kb to a 250 kb region), with 1.6 kb and 800 bp resolution respectively. Standard colormap scheme that uses the shades of red from white (no detectable interactions) to black (maximum interactions detected) in log10 scale. **(B)** Almost no loops are detected upon cohesin depletion, while condensin depletion presents a small reduction in the number of loops. Bar chart shows the loop number called by the HiCCUPS program in wild-type (*WT*), cohesin Mcd1p-depleted (*MCD1-AID*), and condensin Brn1p-depleted (*BRN1-AID*) cells. **(C)** Genome-wide analysis confirms loop signal is gone in cohesin-depleted cells and slightly reduced upon depletion of condensin. Heatmaps were plotted with 200 bp resolution data for wild-type (*WT*), cohesin Mcd1p-depleted (*MCD1-AID*), and condensin Brn1p-depleted (*BRN1-AID*), and cohesin and condensin depleted (*MCD1-AID BRN1-AID)* cells in +/- 5-kb regions surrounding the wild-type loop anchors. Numbers in the corners represent the fold-change of the signal enrichment of the center pixel over the indicated corner pixels (14^2 pixels). The contact map was normalized by matrix balancing and distance, using a diverging colormap with positive signal enrichment in red and negative signals in blue (gradient of normalized contact enrichment is in log2). **(D)** Cohesin depletion shows fewer contacts in the size-region corresponding to the size of loops, while condensin depletion does not. Interactions-versus-distance decaying curve shows the normalized contact density (y-axis) against the distance between the pair of crosslinked nucleosomes from 100 bp to 1 Mb (x-axis) for wild-type (*WT*) versus condensin Brn1p-depleted (*BRN1-AID*) left, or versus cohesin Mcd1p-depleted (*MCD1-AID*). **(E)** Cohesin depletion results in more inter-chromosomes contacts. Bar chart shows the number of inter-chromosomes contacts in wild-type (*WT*), cohesin Mcd1p-depleted (*MCD1-AID*), condensin Brn1p-depleted (*BRN1-AID*), and cohesin and condensin depleted (*MCD1-AID BRN1-AID).*

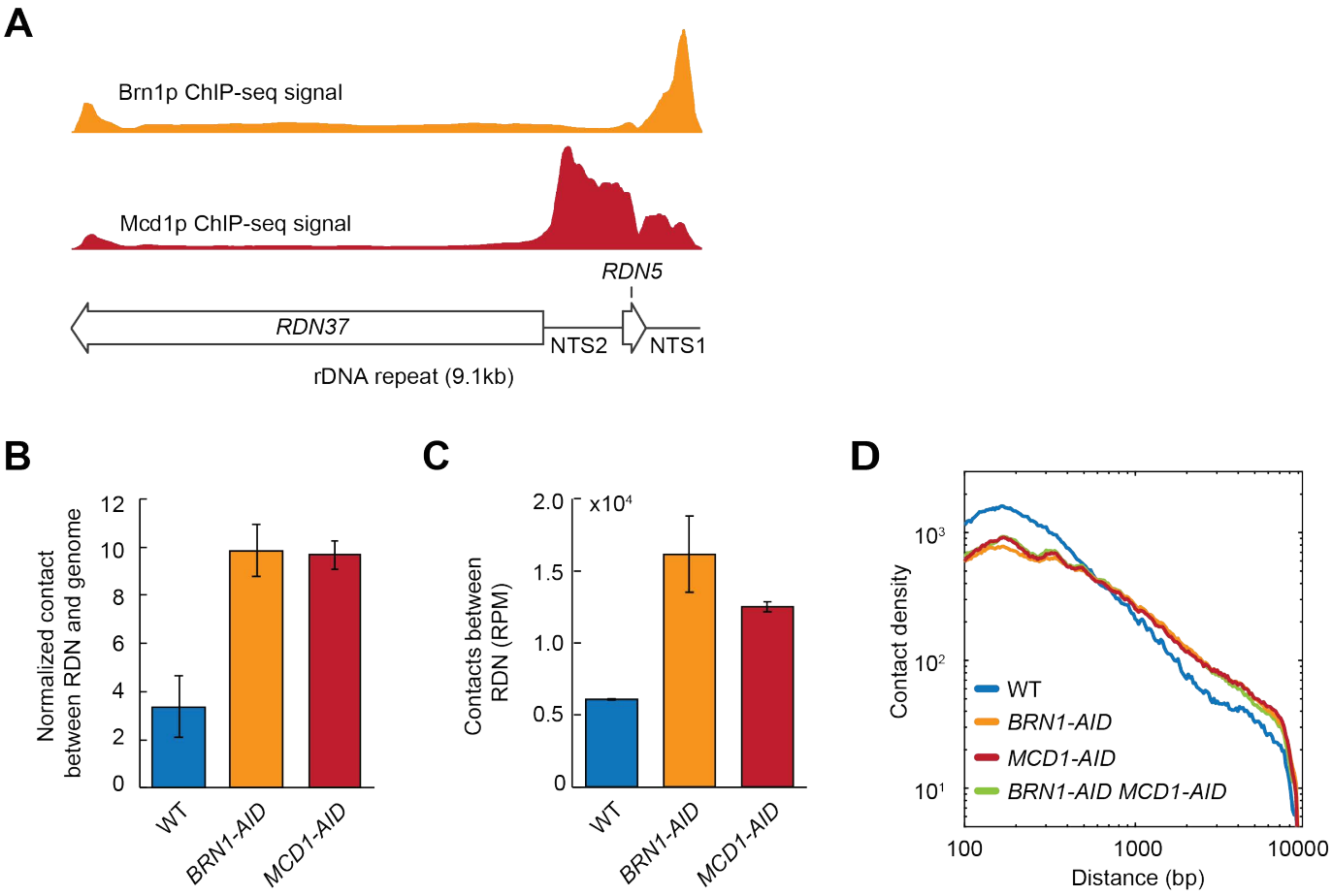

Figure 2—figure supplement 2. Ribosomal DNA (RDN) structure in mitosis is dependent on cohesin and condensin.

(A) Cohesin and Condensin accumulate in the 3' region of each rDNA repeat. ChIP-seq signal of condensin (Brn1p) in yellow shows how condensin accumulates on the NTS1 region. ChIP-seq cohesin (Mcd1p) in red shows cohesin accumulation on the NTS1 and 2. Below a model for the genomic organization of the rDNA repeat, where each repeat is made of two transcribed regions (RDN37 and RDN5) and two non-transcribed regions (NTS1 and NTS2). **(B)** Cohesin and condensin depletion makes the rDNA less isolated from the rest of the genome. Normalized contacts between the rDNA and the rest of the genome in wild-type (*WT*), condensin Brn1p-depleted (*BRN1-AID*), cohesin Mcd1p-depleted (*MCD1-AID*). **(C)** Cohesin and condensin depletion increases the number of contacts between the RDN. Reads per million mapped reads (RPM) contacts between rDNA in wild-type (*WT*), condensin Brn1p-depleted (*BRN1-AID*), cohesin Mcd1p-depleted (*MCD1-AID*). **(D)** Cohesin and condensin depletion shows more long-range contacts on RDN. Interactions-versus-distance decaying curve shows the normalized contact density (y-axis) against the distance between the pair of crosslinked nucleosomes from 100 bp to 10000 bp (x-axis) for wild-type (*WT*), condensin Brn1p-depleted (*BRN1-AID*), cohesin Mcd1p-depleted (*MCD1-AID*), and condensin and cohesin depleted cells (*BRN1-AID MCD1-AID)*.

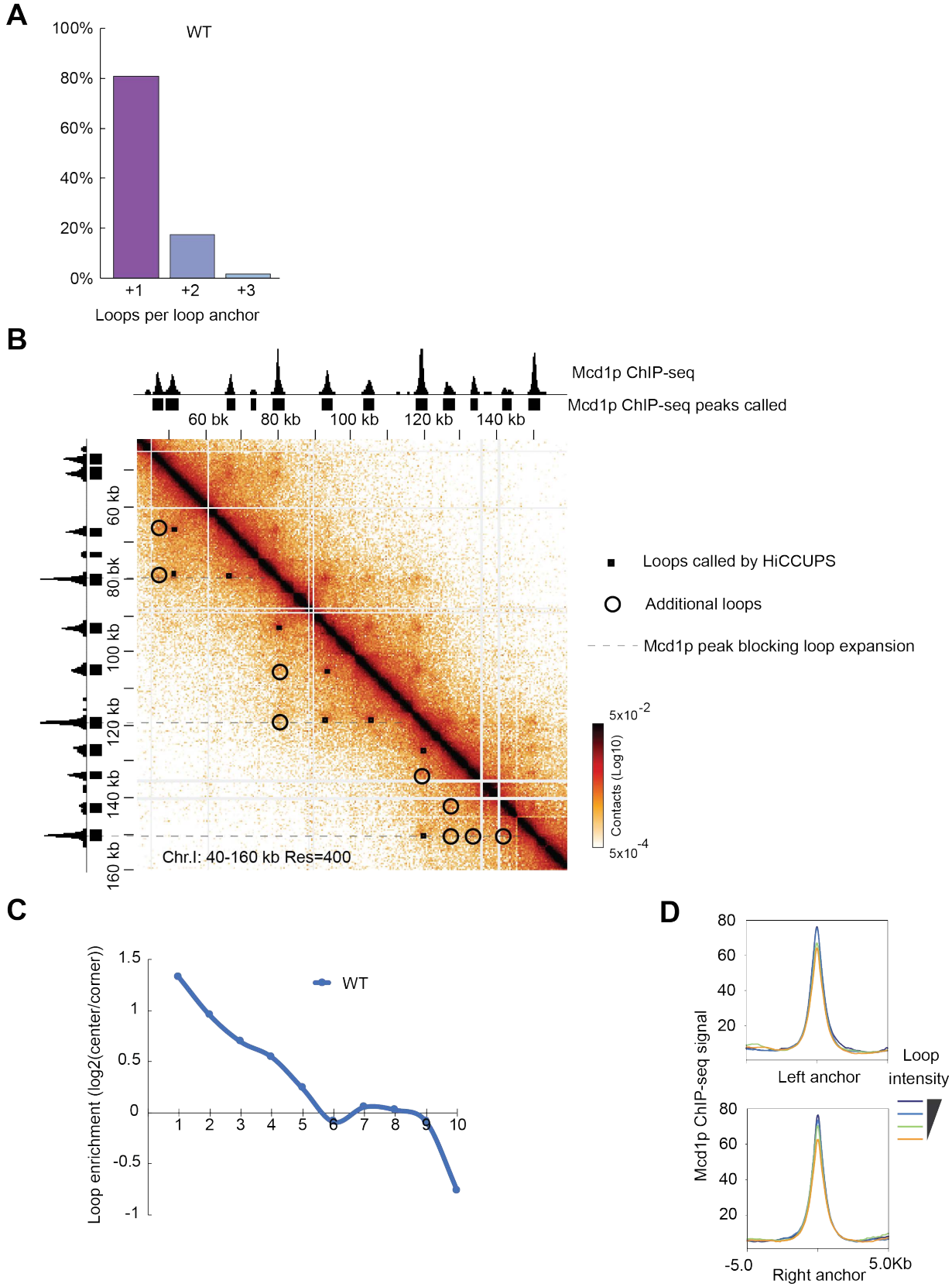

Figure 3—figure supplement 1. Cohesin-dependent organization of loops.
(A) Genome-wide analysis confirms loop expansion in wild-type. Bar chart shows the percentage of the number of loops per anchor in wild-type (*WT*) arrested in mitosis. **(B)** Around half of the visible loops are missed by HiCCUPS loop calling program. Contact map showing the interaction in the 40-160 kb region of chromosome I overlay with the tracks for Mcd1p ChIP-seq signal and peaks. Squares indicate loops called by HiCCUPS. Circles indicate visibly distinct loops missed by HiCCUPS. Dashed lines indicate the position of barriers that insulate from loop expansion. **(C)** Loop signal is detected till the +5 loop anchors interval genome-wide. Quantification of the heatmap analysis in figure 3D. The chart shows the loop enrichment (Log2 of the ration of the loop signal in the center of the heatmap divided for the background signal in the corner) on the y-axis present at each CAR interval (x-axis) in wild-type (*WT*) cells in mitosis. **(D)** Loop intensity correlates with the intensity of Mcd1p ChIP-seq signal at the corresponding loop anchors. Loop intensity was sorted into quartiles from high to low. Mcd1p ChIP-seq signal was plotted against the loop anchors at the center.

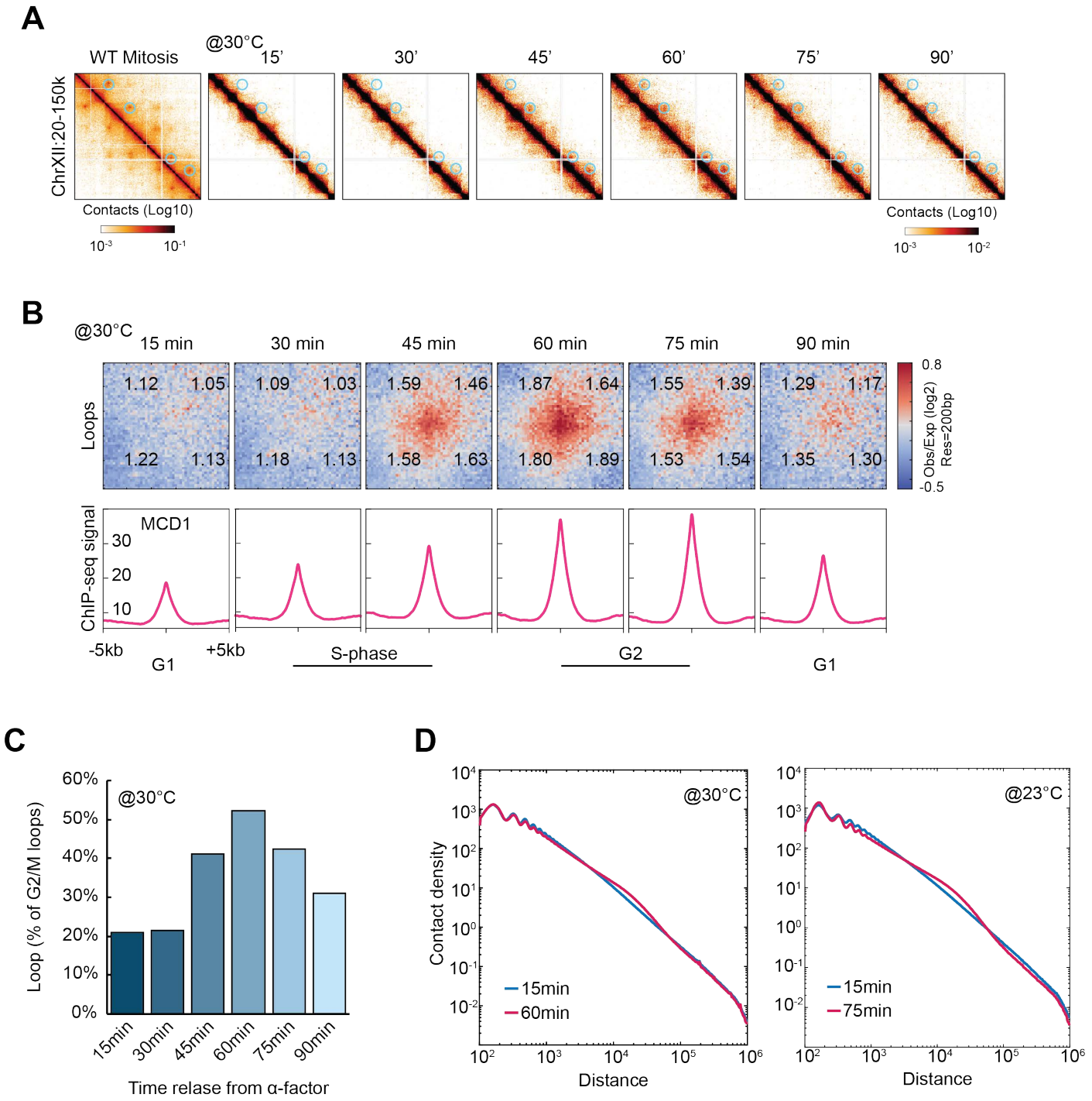

Figure 4—figure supplement 1. Loop formation during the cell cycle.
(A) Loops detected during the time course are less defined on the contact map. Snapshots for cells arrested in mitosis (left) and then each time point after G1 release at 30°C. It represents the chromatin interaction in the 20-150 kb region of chromosome XII. Note that snapshot for the time points is in a higher color contrast than the mitotically-arrested sample for a better loop visualization. **(B)** Chromatin loops emerge upon cohesin deposition during DNA replication. The figure shows Micro-C (top) and Mcd1p ChIP-seq (bottom) data across a time course after release from G1 arrest (15 to 90 minutes) at 30°C. Heatmaps were plotted with 200 bp data resolution across a time course in +/- 5-kb regions surrounding the loop anchors identified in the mitotically arrested wild-type data. Average Mcd1p peak intensity was plotted across +/- 5 kb regions around the center of loop anchors at each time point. **(C)** Loop formation peaks in G2 (60-min time point after G1 release at 30°C). Bar chart represents the percentage of loop numbers at each time point compared to the number of loops found upon mitotic arrest. **(D)** G2 cells present more contacts in the loop size-range. Interactions-versus-distance decaying curve shows the normalized contact density (y-axis) against the distance between the pair of crosslinked nucleosomes from 100 bp to 1 Mb (x-axis) for 15 min (G1) versus 60 min (G2) at 30°C (left panel). Decaying curve comparing 15 min (G1) versus 75 min (G2) at 23°C (right panel).

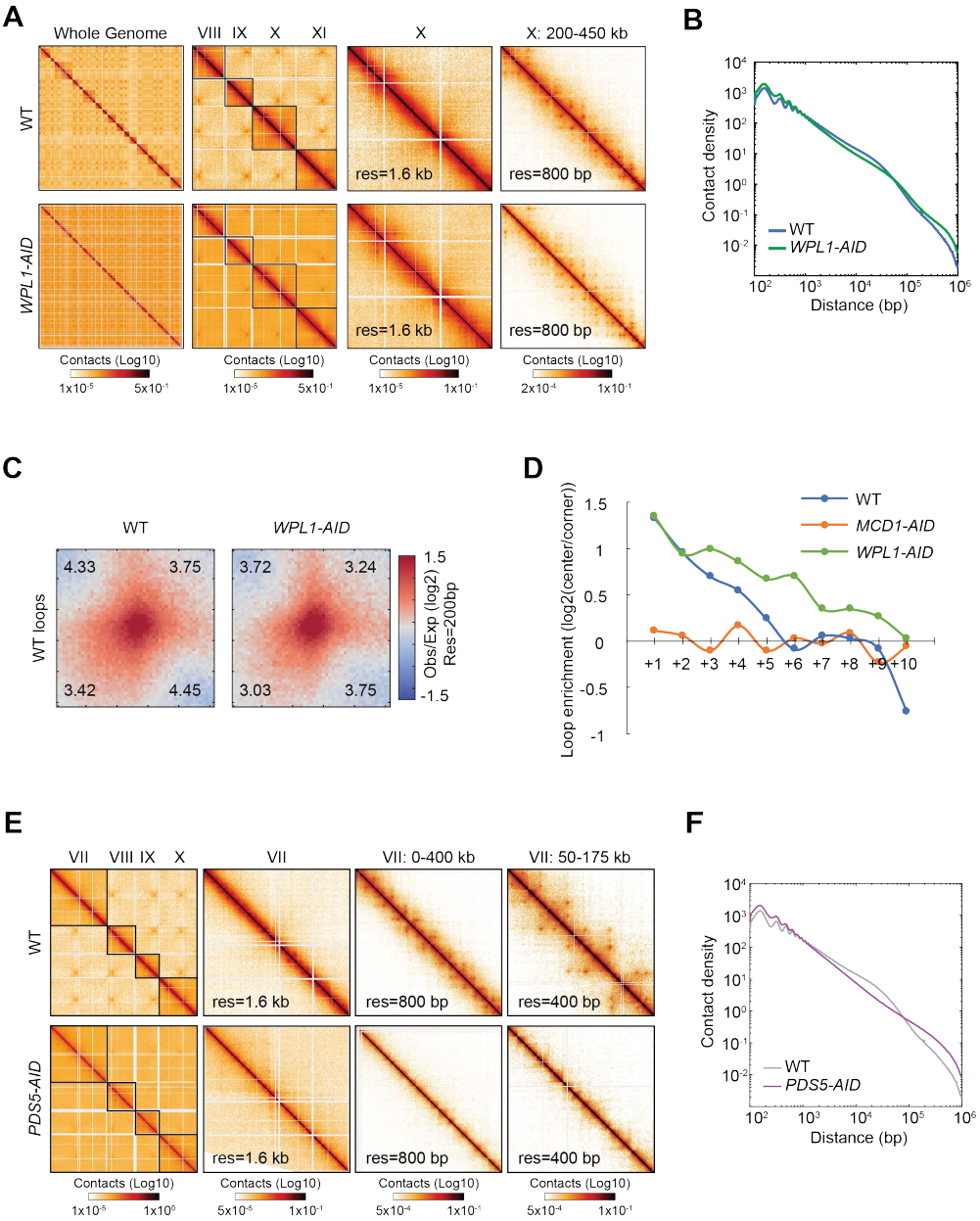

Figure 5—figure supplement 1. Wpl1p- and Pds5p-depletion alters the pattern of loops genome-wide.
(A) Wpl1p depleted-cells present more loops and more loop expansion. Contact maps from mitotically arrested cells produced with Micro-C on wild-type (*WT*), cohesin Wpl1p-depleted (*WPL1-AID*). Contact maps show contacts between the whole genome (first column), followed by contacts from chromosomes VIII to XI at 6.4 kb resolution (second column). The following contact maps show chromosome X and a zoomed-in region (from the full 745 kb to a 250 kb region), with 1.6 kb and 800 bp resolution respectively. Standard colormap scheme that uses the shades of red from white (no detectable interactions) to black (maximum interactions detected) in log10 scale. **(B)** Distribution of contacts upon Wpl1p-depletion. Interactions-versus-distance decaying curve shows the normalized contact density (y-axis) against the distance between the pair of crosslinked nucleosomes from 100 bp to 1 Mb (x-axis) for wild-type (*WT*) versus Wpl1p-depleted (*WPL1-AID*) cells. **(C)** The loop signal at wild-type loops is still present upon Wpl1p-depletion. Heatmaps were plotted with 200 bp data resolution for wild-type (*WT)* and Wpl1p-depleted (*Wpl1-AID)* cells in +/- 5-kb regions surrounding the wild-type loop anchors. **(D)** Loop signal is detected till the +10 loop anchors interval upon Wpl1p-depletion. Quantification of the heatmap analysis in figure 5D for Wpl1p-depleted (*WPL1-AID*) cells compared to wild-type (*WT*) and cohesin-depleted (*MCD1-AID*). The chart shows the loop enrichment (Log2 of the ration of the loop signal in the center of the heatmap divided for the background signal in the corner) on the y-axis present at each CAR interval (x-axis). **(E)** Pds5p depleted-cells present no loops on chromosome arms. Contact maps from mitotically arrested cells produced with Micro-C on wild-type (*WT*), Pds5p-depleted (*PDS5-AID*). Contact maps show contacts between chromosomes VII to X at 6.4 kb resolution (first column). The following contact maps show chromosome VII and zoomed-in regions (from the full 1090 kb to a 125 kb region), from 1.6 kb to 400 bp resolution. Standard colormap scheme that uses the shades of red from white (no detectable interactions) to black (maximum interactions detected) in log10 scale. **(F)** Pds5p-depleted cells lose contact in the loop-size range. Interactions-versus-distance decaying curve shows the normalized contact density (y-axis) against the distance between the pair of crosslinked nucleosomes from 100 bp to 1 Mb (x-axis) for wild-type (*WT*) versus Pds5p-depleted (*PDS5-AID*) cells.

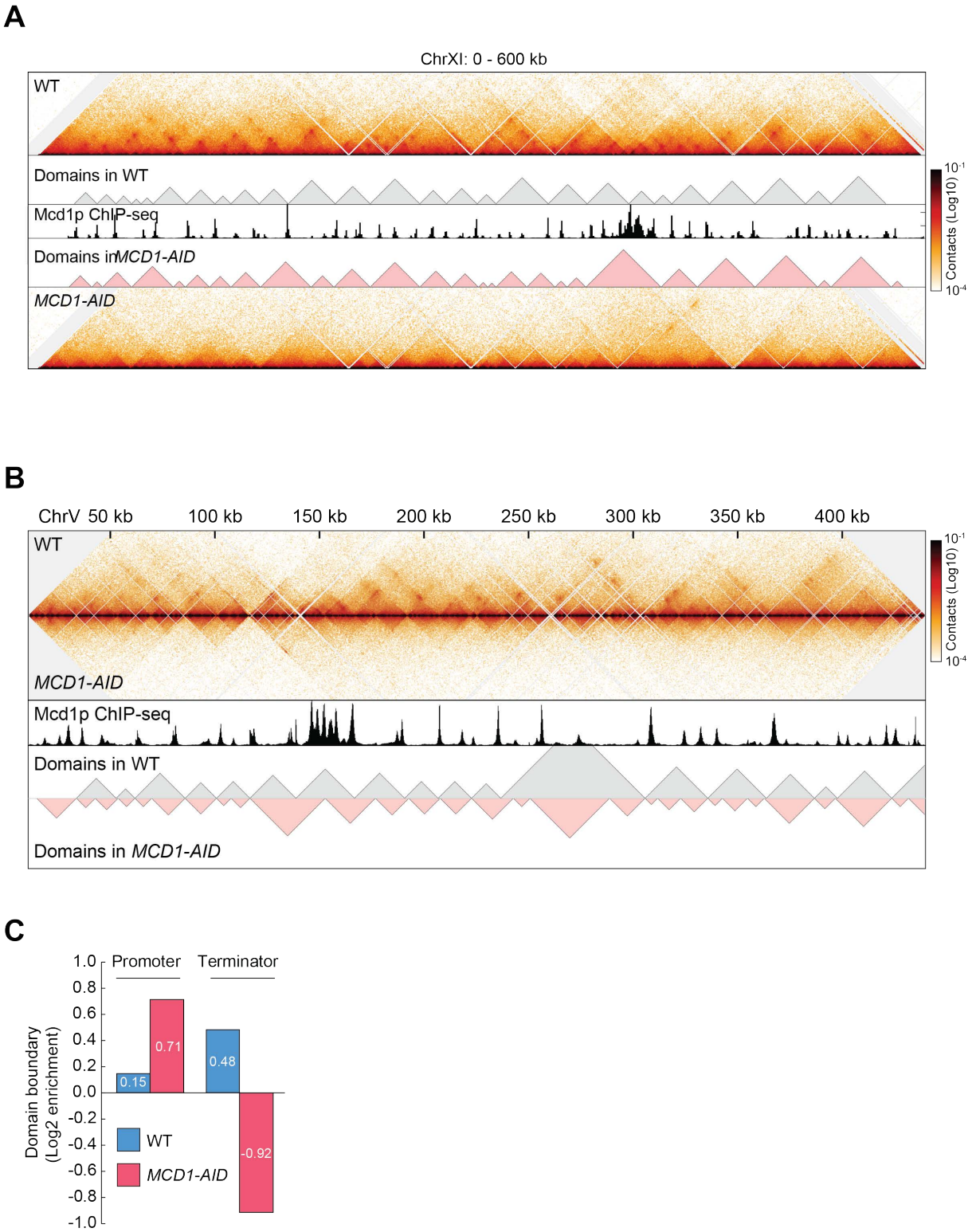

Figure 6—figure supplement 1. Cohesin depletion alters the chromatin domain landscape.
(A) Chromosome domains are reorganized after cohesin removal. Wild-type (*WT*) (first row) and cohesin depleted cells (*MCD1-AID*) (fifth row) data are plotted as 45°-rotation contact maps across chromosome XI: 0-600 kb region. 1-kb resolution Micro-C data were used for domain calling with the insulation analysis. The boundary-delimited domains in wild type are in grey (second row), and the boundary-delimited domains in cells depleted for cohesin (*MCD1-AID*) are in red (fourth row). Finally, Mcd1p ChIP-seq signal (third row) is overlaid with the contact maps in the same region. **(B)** Second snapshot to show the different domain organization upon cohesin depletion. Wild-type (*WT*) (first row) and cohesin depleted cells (*MCD1-AID*) (second row) data are plotted as 45°-rotation contact maps across chromosome V: 0-450 kb region. 1-kb resolution Micro-C data were used for domain calling with the insulation analysis. Mcd1p ChIP-seq signal (third row) is overlaid with the contact maps in the same region. The boundary-delimited domains in wild type are in grey (second row), and the boundary-delimited domains in cells depleted for cohesin (*MCD1-AID*) are in red (fourth row). **(C)** CAR domain boundaries are enriched at terminators, while domains in cohesin-depleted cells are enriched at promoters. Bar chart shows the log2 enrichment of domain boundaries from wild-type (*WT*) in blue and cohesin-depleted cells (*MCD1-AID*) in red, at promoter or terminator.

Materials and Methods

Yeast strains and culture conditions

All strains used in this study are derived from the A364A background and their genotypes are listed in Table 1. YEP (yeast extract, peptone, and dextrose) medium was prepared as described previously (Guacci et al. 1997a). Cells were grown to early log phase (OD600 0.1–0.2) overnight at 23°C and arrested in G1 using the pheromone α factor at a concentration of 10 µM (Sigma Aldrich T6901-5MG). If indicated, auxin was added to a final concentration of 500 µM to deplete AID-tagged proteins after a 2.5-h arrest. Cells were released from G1 by washing with YPD containing auxin (if indicated) and 0.15 mg/mL pronase E (Sigma Aldrich) three times, and once with YPD plus auxin. After the last wash, cells were resuspended in YPD medium containing auxin and 15 µg/mL nocodazole (Sigma Aldrich) to arrest them in mitosis. Cultures were then once again incubated for 3 h at 23°C. For the time course, cells were grown to early log phase (OD600 0.1–0.2) overnight at 23°C or 30°C and arrested in G1 using the pheromone α factor at a concentration of 10 µM (Sigma Aldrich T6901-5MG). Cells were released from G1 by washing with YPD containing auxin (if indicated) and 0.15 mg/mL pronase E (Sigma Aldrich) three times, and once with YPD. After the last wash, cells were resuspended in YPD medium with no drugs and time points were collected every 15min.

Chromatin Immunoprecipitation followed by sequencing (ChIP-seq)

Cells were grown and arrested at 23°C as described in the previous paragraph. ChIP-seq was performed as previously described (Costantino and Koshland, Mol Cell 2018). Briefly, 1x10^10 cells of exponentially growing cells (in 0.5 L of YEP+ 2% glucose) were fixed with paraformaldehyde (final 1%) for 1h. Glycine was added to stop the reaction at 0.125M for 10'. Cells were collected by centrifugation and washed once with PBS 1X buffer, once with TE 1X buffer and stored at -80C. Frozen cell pellets were resuspended in FA buffer (1% Triton X-100, 0.1% sodium deoxycholate,0.1% SDS, 50 mM HEPES, 150 mM NaCl, 1 mM EDTA) and disrupted three times using a FastPrep-24 5G instrument for 40 sec (6.0 m/sec each) (MP Bio). Chromatin was sheared 10 × 30 sec on/30 sec off with a Bioruptor Pico (Diagenode). Supernatant with chromatin extract was isolated after a 10 minutes centrifugation at 14.000g at 4°C. Immunoprecipitation of DNA-protein was performed using 4 µL of the polyclonal rabbit anti-Mcd1p (Covance Biosciences) overnight at 4°C. Antibody-bound lysates were incubated with 120 µL Protein A dynabeads (Invitrogen 10001D) for 1h. Beads were then washed and the DNA eluted according to standard ChIP protocols: 5 successive washes with 1X FA, 1X FA with
0.5M NaCl, Lithium chloride detergent (0.25M LiCl, 0.5% NP-40, 0.5% Sodium deoxycholate, 1mM EDTA, and 10mM Tris-HCl), and finally twice with TE buffer. DNA was then eluted from the beads with 300ml of Elution buffer (1% SDS, 0.1M NAHCO3). To ensure antibody is fully removed samples are treated with 1ml proteinase K (20mg/ml) for 1 hour at 42 while shaking at 1000 rpm, and the ssDNA was then isolated using QIAGEN PCR purification kit (28104 QIAGEN) and eluted in 20ml low EDTA TE. The library was prepared using the Accel-NGS 1S Plus DNA Library Kit (Swift Bioscience) following the manufacturer protocol. Libraries were
sequenced using Illumina Hiseq 4000. The sequencing files were aligned to the SacCer3 yeast genome using Bowtie2 tool and bigwig files were normalized for number of reads. Identified regions of enrichment were called using MACS, with default settings.

ChIP-seq data are accessible from the GEO repository accession number GSE151416.

Yeast Micro-C assay

We used the Micro-C protocol reported in (Hsieh et al. 2016b) with some minor modifications. Yeast cultures in the indicated conditions were immediately crosslinked with 3% formaldehyde for 15 minutes at 30°C, then quenched with 250mM glycine at room temperature for 5 minutes. Crosslinked yeast cells were pelleted by centrifugation at 4000 rpm at 4°C for 5 minutes and washed once with deionized water. Pelleted yeast cells were then spheroplasted with 250 ug/mL Zymolyase (MP08320932) in the Buffer Z (1M sorbitol, 50mM Tris-HCl pH 7.4, 10mM β-mercaptoethanol) at 30°C with vigorously shaking. Complete spheroplasting usually takes up to 40 to 60 minutes at which the milky solution turns to translucent, or the OD550 value drops to about half. Spheroplasts were washed once by 1X ice-cold PBS and then spun down at 4000 rpm at 4°C for 2 minutes. Pellets were resuspended in the DSG crosslinking solution (3mM disuccinimidyl glutarate (ThermoFisher #20593) in 1X PBS and incubated at 30°C for 40 minutes with gentle shaking. Crosslinking reaction was quenched with 400mM glycine at room temperature for 5 minutes. Cells were pelleted by centrifugation at 4000 rpm at 4°C for 10 minutes and washed once with ice-cold PBS. Crosslinked cells can be stored at -80℃ for few months or proceed to chromatin fragmentation immediately. We note that using freshly made formaldehyde and DSG solution is critical to generate high-quality Micro-C data.

Crosslinked cells were permeabilized with MB1 (50mM NaCl, 10mM Tris-HCl pH 7.5, 5mM MgCl2, 1mM CaCl2, 0.5mM Spermidine, 1.43mM β-mercaptoethanol, 0.005% NP-40) on ice for 5 minutes. Chromatin was fragmented into ~90% mononucleosome and ~10% dinucleosome with Micrococcal Nuclease (MNase) (Worthington Biochem #LS004798). We recommend titrating the MNase digesting condition for each sample. Typically, we treat cells with various pre-titrated MNase concentrations and then incubate them at 37°C for 10 minutes with vigorously mixing. MNase reaction was inactivated by adding 2.5mM EGTA and incubated at 65°C for 10 minutes. Chromatin was pelleted by centrifugation at 16000g at 4°C for 5 minutes and washed twice with ice-cold MB2 (50mM NaCl, 10mM Tris-HCl pH 7.5, 10mM MgCl2). We note that MNase titration to yield 90% monomer / 10% dimers reduces un-digested (un-ligated) dimers contamination in Micro-C data.

MNase-digested fragments were then subject to the customized three-step end-repair protocol. First, chromatin was resuspended in the end-repair buffer (50mM NaCl, 10mM Tris-HCl pH 7.5, 10mM MgCl2, 100µg/mL BSA, 2mM ATP, 5mM DTT) and phosphorylated the 5'-ends with 25 units of T4 Polynucleotide Kinase (NEB #M0201) at 37°C for 15 minutes. Second, treating chromatin with 25 units of DNA Polymerase I, Large (Klenow) Fragment (NEB #M0210) in the absence of dNTPs at 37°C for 15 minutes allows the Klenow enzyme using its 3'-to-5' exonuclease activity to convert the mixed types of nucleosomal ends to the cohesive ends. Tight binding and chemical crosslinking between DNA and nucleosome are supposed to prevent the Klenow enzyme's 3'-to-5' exonuclease activity from chewing nucleosomal DNA all the way through. Third, Klenow enzyme's polymerase activity repairs the nucleosomal DNA ends to the blunt and ligatible ends upon the supplement of dNTPs including 66uM dTTP, dGTP (NEB #N0446), biotin-dATP (Jena Bioscience #NU-835-BIO14), and biotin-dCTP (Jena Bioscience #NU-809-BIOX) in 1X T4 DNA ligase reaction buffer (NEB #B0202). The reaction was incubated at 25°C for 45 minutes with interval mixing and then inactivated with 30mM EDTA at 65°C for 20 minutes. Chromatin was pelleted by centrifugation at 16000g at 4°C for 5 minutes and washed once with ice-cold MB3 (50mM Tris-HCl pH 7.5, 10mM MgCl2).

Biotinylated-nucleosomes were then subjected to the proximity ligation reaction with 5000 cohesive end units (CEU) of T4 DNA ligase (NEB #M0202) in 1X T4 DNA ligase reaction buffer (NEB #B0202) at room temperature for at least 1.5 hours with slowly shaking. After ligation, biotin-dNTPs at the DNA termini were removed with 500 units of Exonuclease III (NEB #M0206) in 1X NEBuffer 1 (NEB #B7001) at 37°C for 15 minutes. Samples were then reverse crosslinked with 1X proteinase K solution (500 ug/uL Proteinase K (ThermoFisher #AM2542), 1% SDS, 0.1 ug/uL RNaseA) at 65°C overnight. DNA was extracted by the standard Phenol:Chloroform:Isoamyl Alcohol (25:24:1) and ethanol precipitation procedure. DNA was then loaded and purified on ZymoClean column. Purified DNA was separated on a 3% NuSieve GTG agarose gel (Lonza #50081). The gel band corresponding to size of dinucleosomal DNA (~250 to 350bp) was cut and purified with Zymoclean Gel DNA Recovery Kit (Zymo #D4008). We note

that the size-selection for DNA larger than 200bp greatly reduces the ratio of unligated monomer in Micro-C data.
Micro-C sequencing library was generated by using NEBNext Ultra II DNA Library Prep Kit for Illumina (NEB #E7645) with some modifications. Purified DNA was end-repaired using End-it from Lucigen. 17.5ul DNA was added to 2.5ul 10X end-it buffer, 2.5ul 10x ATP and 2.5ul dNTP 10x, and finally 0.5 end-it enzyme was added. The mix was incubated at 25°C for 45min and at 70°C fro 10min. Then the Biotinylated-DNA was captured by Dynabeads MyOne Streptavidin C1 beads (ThermoFisher #65001) in 1X BW buffer (5mM Tris-HCl pH 7.5, 0.5mM EDTA, 1 M NaCl) at room temperature for 20 minutes with gentle rotation. DNA-conjugated beads were washed twice with 1X TBW buffer (0.1% Tween20, 5mM Tris-HCl pH 7.5, 0.5mM EDTA, 1 M NaCl) at 55°C for 5 minutes with vigorously shaking, rinsed once with Tris buffer (10mM Tris-HCl pH 7.5), and then resuspended in Tris buffer. We then performed "on-bead" end-repair / A-tailing and adapter ligation following the NEB protocol. Adapter-ligated DNA was washed once with 1X TBW and rinsed once with Tris buffer before PCR amplification. Micro-C library was generated by using KAPA HiFi HotStart ReadyMix (Roche #KK2601) or Q5 High-Fidelity 2X Master Mix (NEB #E7645) with commercial recommended conditions. We recommend using a minimal PCR cycle to reduce PCR duplicates, typically ranging from 8 to 12 cycles that can generate high-quality data for yeast samples. Prior to sequencing, purifying the library twice with 0.85X AMPure XP beads (Beckman #A63880) can eliminate primer dimers and adapters. We used Illumina 100-bp paired-end sequencing (PE100) to obtain ~50M reads for each replicate in this study.

Micro-C data are accessible from the GEO repository accession number GSE151553.

Preprocessing Micro-C data from fastq to contact matrix
Each fastq mate was mapped to the yeast sacCer3 genome independently using Bowtie 2.3.0 (Langmead and Salzberg 2012) with 'very-sensitive-local' mode. Aligned reads were paired by the read name. Pairs with multiple hits, low MAPQ, singleton, dangling end, self-circle, and PCR duplicates were discarded. Contacts shorter than 200bp (unligated monomer) were also removed. Output files containing all valid pairs were used in downstream analyses. Valid Micro-C contact read pairs were obtained from the HiC-Pro analysis pipeline (Servant et al. 2015). The detailed description and code can be found at https://github.com/nservant/HiC-Pro. We recommend checking these quality control statistics before moving forward to the downstream analysis: 1) bowtie mapping rate; 2) reads pairing percentage; 3) ratio of sequencing artifacts; 4) ratio of cis/trans contacts; 5) unligated monomer percentage. If any of the above statistics is not in the optimal range, one might consider checking mapping and filtering parameters or further optimize the Micro-C experiment.
Valid Micro-C contacts were assigned into the corresponding 'pseudo' nucleosome bin. The bin file was pre-generated from the yeast sacCer3 genome by the 100-bp window that virtually resembles the nucleosome resolution. The binned matrix can be stored in HDF5 format as COOL file format by using COOLER package (https://github.com/mirnylab/cooler) (Abdennur and Mirny 2019) or HIC file format by using JUICER package (https://github.com/aidenlab/juicer) (Durand et al. 2016). COOL and HIC are the standard 4DN formats that are compatible with many downstream analysis ecosystems (https://www.4dnucleome.org/). Contact matrices were then normalized by using iterative correction (IC) in COOL files (Imakaev et al. 2012) or Knight-Ruiz (KR) (Knight and Ruiz 2013) in HIC files. Regions with low mappability and high noise were blocked before matrix normalization. We expect that matrix balancing normalization corrects systematic biases such as nucleosome occupancy, sequence uniqueness, GC content, or crosslinking effects (Imakaev et al. 2012). We notice that both normalization methods produce qualitatively equal contact maps. To visualize the contact matrices, we generated a compilation of COOL file with multiple resolutions (100-bp to 12800-bp bins) that can be browsed on the Higlass 3D genome server (http://higlass.io) (Kerpedjiev et al. 2018). In this study, all snapshots of Micro-C or Hi-C contact maps and the 1D browser tracks (e.g., ChIP-seq) were generated by the Higlass browser unless otherwise mentioned.

Genome-wide contact decaying curve analysis

We only used intra-chromosomal contact pairs to calculate the contact probability in bins with exponentially increasing widths from 100 bp to 1 Mb. Contacts with a distance shorter than 100 bp were removed from the analysis to minimize noise introduced by self-ligation or undigested DNA products. Decaying curves in this study were normalized to the total number of contact pairs. The orientations of ligated DNA are parsed into "IN-IN (+/-)," "IN-OUT' (+/+)," "OUT-IN' (-/-)," and "OUT-OUT' (-/+)" according to the readouts of Illumina sequencing (Hsieh et al. 2015). "UNI" pairs are the combination of "IN-OUT"" and "OUT-IN" because both orientations are theoretically interchangeable. We plotted the contact decaying curves with the "UNI" orientation in this study unless otherwise mentioned.

Chromatin loop analysis

Loops (focal contact enrichment) in this study were identified by using the HICCUPS algorithm (Rao et al. 2014) in the JUICER package and Chromosight (Matthey-Doret et al. 2020). Loops were called with KR-normalized Micro-C contact matrices at 500-bp resolution, and filtered by a false discovery rate at 0.1 (calling options: -m 4096 -k KR -r 500,500 -f 0.1,0.1 -p 6,8 -i 12,16 -d 2500,2500). Hi-C data from (Schalbetter et al. 2017, 2019; Paldi et al. 2020; Hsieh et al. 2016a) were reanalyzed with the same loop calling option. Apparent false-positive callings (e.g., distance larger than 100 kb) were manually removed. We applied the lists of loop anchor to many downstream analyses by using Bedtools (Quinlan and Hall 2010), including 1) comparison of loop anchors between Micro-C and Hi-C, 2) histogram of loop size, 3) cross-correlation with ChIP-seq data, 4) the number of loops per anchor, etc. We noted that the current loop calling algorithm does not identify all the visible chromatin loops, mostly skipping a subset of distal and weaker loops.

Genome-wide loop intensity was assessed by the aggregate peak analysis (APA) (Rao et al. 2014). We used JUICER (Durand et al. 2016) or coolpuppy (Flyamer et al. 2020) packages to perform the analysis. In brief, loops were centered and piled up on a 10-kb x 10-kb matrix with 200-bp resolution data. The pile-up matrix was then normalized by KR, ICE, or distance, as indicated in the figure legend. Loops close to the diagonal were excluded or normalized by random shift to avoid distance decay effects. The ratio of loop enrichment was calculated by dividing normalized center contacts in a searching window by the normalized corner submatrices.

We used the same approach to analyze the genome-wide target-centered loop intensity. Instead of aggregating at the intersection of loop anchors, the matrix is centered at the paired MCD1 ChIP-seq peaks. The pairs are selected for the adjacent peaks at distances shorter than 100 kb or the indicated peak intervals. The pile-up matrix was then normalized by KR, ICE, or distance, as indicated in the figure legend.

Chromatin domain analysis

We used insulation score analysis (Crane et al. 2015) from the cooltools package https://github.com/mirnylab/cooltools) to identify sharp changes in chromatin interactions, which typically represent the domain boundaries. To identify kb-scale cohesin-mediated chromatin domains, we analyzed insulation profiles with Micro-C contact matrices at 1-kb resolution and 15-kb searching window. The sliding window scans across the entire genome and assigns the insulation intensity to its corresponding bin. The insulation scores were obtained and normalized as the log2 ratio of the individual score to the mean of the genome-wide averaged insulation score. Chromatin boundaries can be identified by finding the local minima along with the normalized insulation score. Boundaries overlapping with low mappability regions were removed from the downstream analysis.

For aggregate domain analysis (ADA), each domain was rescaled to a pseudo-size by $N_{i,j}=((C_i-D_{start})/(D_{end}-D_{start}), (C_j-D_{start})/D_{end}-D_{start}))$, where $C_{i,j}$ is a pair of contact loci within domain D that is flanked by D_{start} and D_{end}, and $N_{i,j}$ is a pair of the rescaled coordinates. The rescaled domains can be aggregated at the center of the plot with ICE or distance normalization.

TABLE 1: Strains

Strain name	genotype
WT	MATa trp1Δ::pGPD1-TIR1-CaTRP1 lys4::LacO(DK)-NAT leu2-3,112 pHIS3-GFPLacI-HIS3:his3-11,15 ura3-52 bar1
PDS5-AID	MATa PDS5-3V5-AID2-KANMX6 lys4::LacO(DK)-NAT pHIS3-GFP-LacIHIS3::his3-11,15 trp1-1 ura3-52 bar1
WPL1-AID	MATa PDS5-3V5-AID2-KANMX6 lys4::LacO(DK)-NAT pHIS3-GFP-LacIHIS3::his3-11,15 trp1-1 ura3-52 bar1
Condensin-Myc	MATa YCG1-S406-6MYC-KANMX trp1Δ::pGPD1-TIR1-CaTRP1 lys4::LacO(DK)-NAT leu2-3,112 pHIS3-GFPLacI-HIS3:his3-11,15 ura3-52 bar1